

RESEARCH ARTICLE | JULY 20 2021

# Effect of serum starvation on rheology of cell monolayers

Abhimanyu Kiran  ; Chandra Shekhar  ; Manigandan Sabapathy; Manoranjan Mishra  ; Lalit Kumar  ; Navin Kumar; Vishwajeet Mehandia  



*Physics of Fluids* 33, 071908 (2021)

<https://doi.org/10.1063/5.0050984>

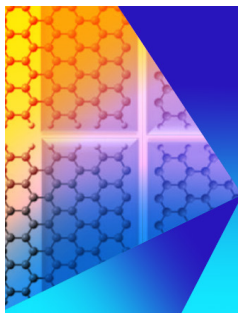


View  
Online



Export  
Citation

CrossMark



**Physics of Fluids** Journal of Applied Physics

Special Topic: Recent Advances in Fluid Mechanics and Nanoelectronics: Memorializing ICRAFNM-2023

**Submit Today!**



# Effect of serum starvation on rheology of cell monolayers

Cite as: Phys. Fluids **33**, 071908 (2021); doi: [10.1063/5.0050984](https://doi.org/10.1063/5.0050984)

Submitted: 21 March 2021 · Accepted: 1 July 2021 ·

Published Online: 20 July 2021



View Online



Export Citation



CrossMark

Abhimanyu Kiran,<sup>1</sup>  Chandra Shekhar,<sup>2</sup>  Manigandan Sabapathy,<sup>2</sup> Manoranjan Mishra,<sup>3</sup>  Lalit Kumar,<sup>4</sup>   
Navin Kumar,<sup>1</sup> and Vishwajeet Mehandia<sup>2,a)</sup> 

## AFFILIATIONS

<sup>1</sup>Department of Mechanical Engineering, Indian Institute of Technology Ropar, Rupnagar, Punjab 140001, India

<sup>2</sup>Department of Chemical Engineering, Indian Institute of Technology Ropar, Rupnagar, Punjab 140001, India

<sup>3</sup>Department of Mathematics, Indian Institute of Technology Ropar, Rupnagar, Punjab 140001, India

<sup>4</sup>Department of Energy Sciences and Engineering, Indian Institute of Technology Bombay, Powai, Mumbai, Maharashtra 400076, India

<sup>a)</sup>Author to whom correspondence should be addressed: [vishwajeet@iitrpr.ac.in](mailto:vishwajeet@iitrpr.ac.in)

## ABSTRACT

The rheological properties of cells and tissues are central to embryonic development and homeostasis in adult tissues and organs and are closely related to their physiological activities. This work presents our study of rheological experiments on cell monolayer under serum starvation compared to healthy cell monolayer with full serum. Serum starvation is one of the most widely used procedures in cell biology. However, the effect of deprivation of serum concentration on the material properties of cells is still unknown. Therefore, we performed macro-rheology experiments to investigate the effect of serum starvation on a fully confluent Madin–Darby Canine Kidney cell monolayer. The material properties, such as linear and non-linear viscoelastic moduli, of the monolayer, were measured using oscillatory shear experiments under serum-free [0% fetal bovine serum (FBS)] and full serum (10% FBS) conditions. Our results indicate that a serum-starved cell monolayer shows a different rheological behavior than a healthy cell monolayer. The loss and storage moduli decrease for the step-change in oscillatory strain amplitude experiments for a serum-starved cell monolayer and do not recover fully even after small deformation. In comparison, a healthy cell monolayer under full serum condition remains flexible and can fully recover even from a large deformation at higher strain. The effect of adhesion due to fibronectin was also studied in this work, and we found a significant difference in slip behavior for cell monolayer with and without serum.

Published under an exclusive license by AIP Publishing. <https://doi.org/10.1063/5.0050984>

## I. INTRODUCTION

The mechanical properties of the active gels, cells, and tissues have been an emerging field of research over the past few decades. The deformability is one of the crucial features of the cells and tissues that are well-acknowledged but poorly understood.<sup>1</sup> Most of the studies report the rheology using micro-rheology techniques of a single cell<sup>2–7</sup> or cell monolayers.<sup>8–10</sup> The micro-rheology techniques include active force probe optical/magnetic tweezers, passive two-point bead tracking via image-based software, and localized dynamic material deformation through an atomic force microscope (AFM). On the other hand, the macro-rheology is usually performed using an oscillatory rheometer.<sup>11–13</sup> The material properties reported by micro-rheology techniques at a cellular or subcellular levels underestimate the bulk properties of cells and tissues<sup>14,15</sup> because the cells are highly heterogeneous, so the viscoelastic parameters obtained from micro-rheology experiments are

local. On the other hand, the macro-rheology can probe the bulk properties, averaging out the heterogeneities for one cell and over a large collection of cells in the monolayers.<sup>12,13</sup>

The living cells are highly complex machines on the planet as they can remodel their cytoskeleton (CSK) to perform various functions like spreading, growth, migration, division, contraction, and metastasis.<sup>16</sup> Hence, instead of structural architecture, the cytoskeleton's dynamic nature fundamentally separates the active cells from passive non-living materials.<sup>17</sup> Further, the disruption of the cell's CSK dynamics via drugs<sup>8,18–20</sup> or mechanical distending<sup>21,22</sup> changes the rheological properties of the cells. As per the well-established literature, two fundamental principles that govern the properties of cells are (1) the pre-existing tension (pre-stress) borne by the cytoskeleton and (2) the weak power-law response of cells to externally applied stress.<sup>23</sup> Ingber's model describes the cell pre-stress,<sup>24,25</sup> whereas the soft glass

rheology (SGR) model<sup>26–29</sup> explains the power-law response of the cells. Although both models are quite different from each other, together, they capture the cell's actual response to the applied deformation.<sup>30,31</sup>

The cell monolayer rheology (CMR) is a well-known macro-rheology technique used to investigate the material properties of the cell monolayer. These properties may vary due to the progression of various diseases like cytotoxicity, malignancy, and other abnormalities. Most of the rheological studies of cells were performed on a discrete cell monolayer, where a large number of single fibroblasts or HeLa cells are attached to both plates of the rheometer.<sup>3,12,13</sup> Cell monolayer rheology can probe a vast number of cells and a better average of mechanical properties. This study uses a similar technique as CMR to probe the cell monolayer of Madin–Darby Canine Kidney (MDCK) epithelial cells. These cells form a continuous cell monolayer, unlike the cell monolayer of many disconnected fibroblasts or HeLa cells.<sup>10</sup> For the CMR, we have used a rheo-microscope module of a commercial rheometer.

Further, the micronutrients (proteins and minerals) are essential for regulating cell viability, homeostasis, and DNA metabolic pathways.<sup>32,33</sup> The serum is the only source in the culture media to provide the micronutrients to the cells. Generally, the concentration of the serum is only 10% of the complete media.<sup>34</sup> The lack of micronutrients can cause genomic instability, protein expression variations, disruptions in signaling pathways, and deprivation of growth factors in the cells.<sup>32,33</sup> It should also be noted that the effect of serum starvation depends on the protocol and the cell type.<sup>32,33</sup> With time, the cells consume the micronutrients and their concentration decay in the culture media. Recently, Miyaoka *et al.*<sup>35</sup> performed micro-rheological experiments using AFM on NIH3T3 fibroblasts under serum starvation. In their study, the cells were incubated with 0.1% fetal bovine serum (FBS) for 24 h and then placed in microarray for another 24 h before the AFM study was done. They found that under serum starvation at 0.1% FBS, the storage modulus ( $G'$ ) and loss modulus ( $G''$ ) show a weak power-law behavior with the frequency, but the dependence of loss modulus ( $G''$ ) on frequency increases after  $\leq 10$  Hz. However, from the above study, it is of utmost importance to understand the cell monolayers' bulk mechanical properties with the effects of serum concentration, which is the main objective of our present paper.

In this study, we present the bulk rheology of fully confluent epithelial cell monolayer of MDCK cells with full serum at 10% FBS, and without serum at 0% FBS, using the CMR technique. The cell monolayer was subjected to standard rheological experiments, including (1) oscillatory shear, which comprises amplitude and frequency sweep, (2) large amplitude oscillatory shear (LAOS), and (3) step strain at a specified shear rate to study the recovery of the properties of the cell monolayer.

Our experimental observations reveal that the cell monolayer's rheological properties depend not only on the applied strain but also on the serum concentration. This work aims to investigate the macro-rheology of MDCK cell monolayer and determine the effect of serum starvation on its rheological properties.

## II. MATERIAL AND METHODS

### A. Cell culture

We used Madin–Darby Canine Kidney (MDCK) II epithelial cells, stably transfected with E-Cadherin Green Fluorescent Protein (J. W. Nelson Lab, Stanford University). We cultured these cells in a

growth medium made of 90% Dulbecco's Modified Eagle Medium (DMEM), low glucose (1% g/l), pyruvate (Cat No.: 11885092, ThermoFisher Scientific) containing 10% Fetal Bovine Serum (FBS) and antibiotics at 37 °C in a 5% CO<sub>2</sub> in a humidified incubator. The cells were replated on a rectangular glass-coverslip (Blue star). When the cell monolayer became 90%–100% confluent (Fig. 1), the growth medium was replaced with Gibco Leibovitz's L15 medium (Cat No.: 11415049, ThermoFisher Scientific) with fetal bovine serum (FBS) and antibiotics. Then these cultures were incubated at 37 °C in a 5% CO<sub>2</sub> humidified incubator for 8 h.

Serum-free and full serum conditions were created when the cells are incubated with Gibco Leibovitz's L15 medium with 0% and 10% FBS at 37 °C in a 5% CO<sub>2</sub> humidified incubator for 8 h, respectively. After this, the cells adhered to the coverslip were used for the rheological experiments (Fig. 2).

### B. Experimental setup

The experiments were conducted with the rheo-microscope (microscope module) of the Modular Compact Rheometer (MCR-702) from Anton Paar GmbH, Germany, which has a quartz glass-bottom plate of 65 mm diameter. We used the 25 mm diameter steel probe for the upper plate, which is attached to a 25 mm glass coverslip to ensure a smooth surface. This is done by a polydimethylsiloxane (PDMS) layer deposited using the spin coater on the glass coverslip by operating at 1000 rpm for 1 min. This coated coverslip was then carefully placed onto the upper probe such that no air bubbles get trapped between them. This probe was left at room temperature for 24 h, followed by heating in the oven for 2 h at 65 °C. This procedure glued the glass coverslip with the rheometer's upper steel plate and made its surface smooth. A similar setup was also used for cell monolayer rheology by Chen *et al.*,<sup>11</sup> Fernandez *et al.*,<sup>12</sup> and Dakhil *et al.*<sup>13</sup> in their studies of bulk rheology of a large collection of single cells, such as fibroblasts and HeLa cells. In the present study, we are using a confluent epithelial cell monolayer with cell-cell contacts.

We used fibronectin (F1141, Sigma–Aldrich), an extracellular matrix protein that helps bind the cells to the surface to control the wall slip. The upper plate with glued glass coverslip was dipped in freshly prepared fibronectin for 3 h at 4 °C. The experiments were conducted after keeping this coated upper plate in touch with the cell monolayer for about half an hour.

The two major challenges faced in the thin gap rheometry are the parallelism of the upper and lower plates of the rheometer and the contact of the upper plate with the material (i.e., cell monolayer in our case). We managed to overcome both these difficulties (see Supplementary Information). To ensure the parallelism of the two plates, we first made a few marks on the bottom plate and then focus on those marks using the microscope with a 20× objective (Mitutoyo, G Plan Apo, 20×, NA = 0.28, depth of field = 3.5 μm). We then fix the focus, which in turn fixes the z-direction. Then, we scan the bottom plate marks from the outer diameter to the center of the plate (by changing the x and y positions) and observe whether any defocusing is happening. We did not observe any defocusing (see [supplementary material](#)). This ensures that the bottom plate is flat and horizontal. We repeated the same procedure of focusing on the glass coverslip of the upper plate and scan for any points/areas of defocusing. We did not observe any defocusing of the upper plate's glass coverslip (see

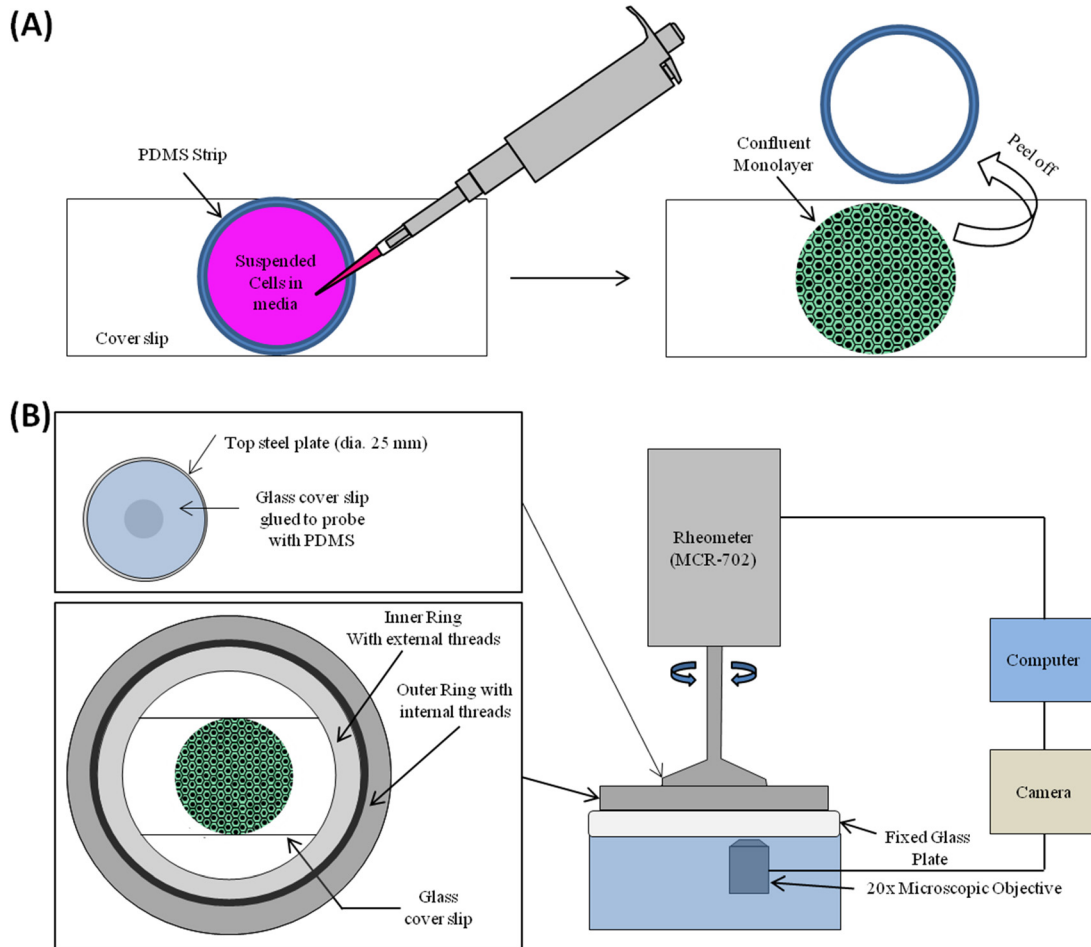


**FIG. 1.** Schematic representation of the setup to perform rheology of the cell monolayer. (a) Preparation of circular cell monolayer using PDMS strip. (b) Setup of rheometer for CMR.

supplementary material), ensuring that the upper glass coverslip is also flat and parallel to the lower glass plate.

We have grown the confluent cell monolayer in a 25 mm diameter circle to fully cover the cell monolayer covered by the upper plate of the rheometer. To grow the circular cell monolayer, we created a circular well using the PDMS ring of the inner diameter of 25 mm on the rectangular coverslip as shown in Figs. 1(a) and 2(a). The cells were seeded in this well and placed in the incubator (at 37 °C in a 5% CO<sub>2</sub>). When the fully confluent monolayer is formed, the old media was removed, and the cells were prepared for the experiment by supplying the fresh (0% FBS or 10% FBS) media. We supplied the media with 0% FBS for the experiments with serum-starved cell monolayer and incubated the cell monolayer at 37 °C in a 5% CO<sub>2</sub> in a humidified incubator for 8 h. The next step is to remove the PDMS well, containing the cell monolayer, and rinse the attached cell monolayer with serum-free media. Thus prepared, the cell monolayer is now ready for the rheology experiments [Fig. 2(b)]. For the experiments with healthy cells, we incubated the cell monolayer with full serum (10% FBS) media for

8 h, removed the PDMS well, and rinsed it with full serum media before placing it under the rheometer for the rheological study. We removed the PDMS ring when the cell monolayer became confluent [Fig. 2(b)]. The rectangular glass coverslip with cell monolayer is fixed firmly on the glass bottom plate with the help of strong adhesive tapes, which are mounted on the sides as shown in Fig. 2(c). This setup with the rectangular coverslip with circular cell monolayer firmly mounted on the glass-bottom plate is then mounted on the rheometer's microscope module [Fig. 2(d)].

The shear rheology was performed by maintaining the initial normal force exerted by the upper plate on the material at  $\sim 0.1$  N. We then fix the gap between the plates and start the experiment. A small change in normal force is observed during the experiment, but the gap between the plates is maintained. It is complicated to maintain the same gap between different runs of the experiment because of the thin gap between the plates and the complex nature of cell monolayers. The fluctuations in the normal force add the difficulty in maintaining the same gap for repeated experiments. The detailed protocol is given in Supplementary Information.

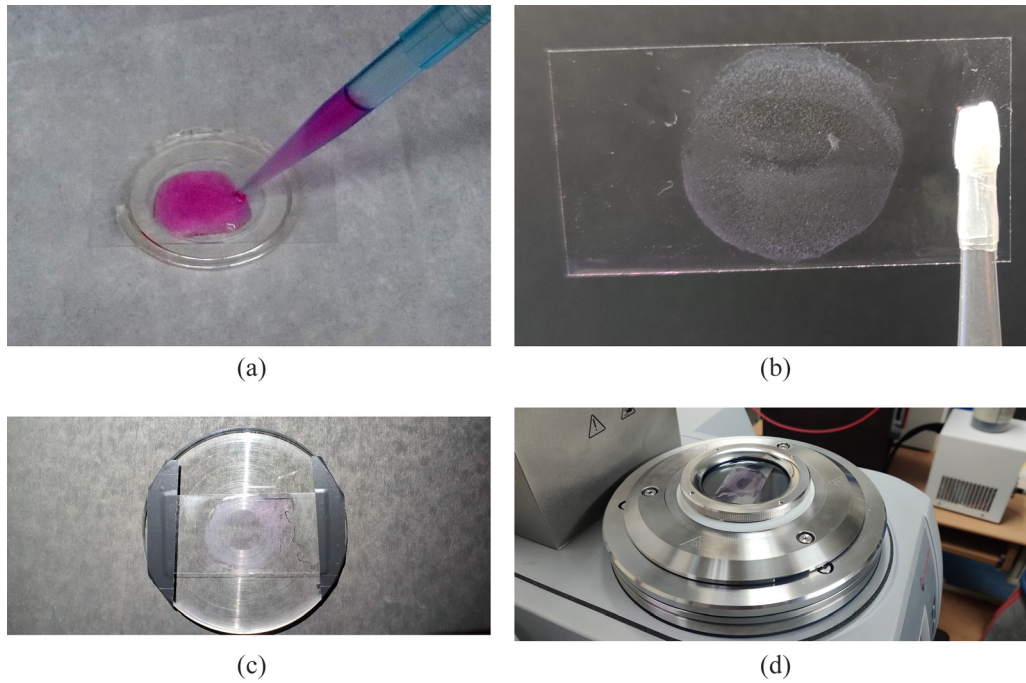


**FIG. 2.** Mounting of cell monolayer on bottom plate: (a) cells are seeded on rectangular glass coverslip with PDMS ring, (b) the circular confluent cell monolayer after the PDMS ring is removed, (c) the rectangular glass coverslip, with circular cell monolayer, is mounted on the bottom glass plate, and (d) the glass bottom plate with coverslip is mounted on the microscope module of the rheometer.

To check whether cells are being sheared, we have stained the actin stress fibers with Texas Red-X phalloidin (ThermoFisher Cat. No. T7471) using the standard protocol<sup>36–38</sup> in the cells before [Fig. 3(a)] and after [Fig. 3(b)] the shearing experiments. The comparison of actin stress fibers before and after the shearing experiments shows that the cells in the monolayer experienced the strain, and the actin fibers are disrupted (Fig. 3). The actin stress fibers are thicker

and randomly oriented in the cell monolayer before shearing as shown in Fig. 3(a), but in Fig. 3(b), which is taken after the shearing experiment, the actin stress fibers are thinner and less abundant in the cell monolayer, indicating that the cell monolayer has experienced the shear during the experiment.

To further improve the confidence for the contact of the upper plate with the cell monolayer, we compressed the monolayer by

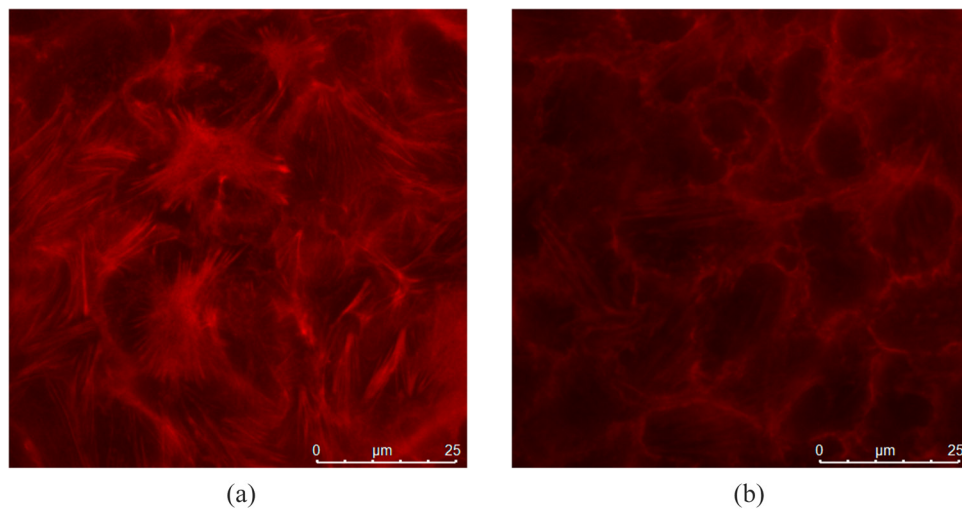


**FIG. 3.** Actin stress (a) before and (b) after the shear experiments. (a) Actin stress fibers before the shear experiment. (b) Actin stress fibers after the shear experiments.

increasing the normal force. Figure 4 shows that as the normal force is increased, the storage modulus  $G'$  increases, but the dependence of the loss and storage moduli on shear strain remains similar. This behavior is observed for the cell monolayer for both cases (a) without serum (FBS = 0%) and (b) with serum (FBS = 10%).

The similar dependence of the storage and loss moduli with shear strain for increasing normal force (or compresses cell monolayer) also indicates that the cells are in contact with the upper plate and being sheared during the experiments.

Following the previous studies of Fernandez *et al.*<sup>12</sup> and Dakhil *et al.*,<sup>13</sup> we conducted all the experiments at 25 °C. The effect of temperature on cell monolayer will be the same for all conditions, i.e., with and without serum. In the current study, we assumed that if the temperature is the same for all conditions, its effect on rheological properties may be the same for all rheological experiments and can be factored out. Also, to maintain the cell number density constant, we observe the confluent cell monolayer under a fluorescence microscope and measure the cell number density. When the cell number density reaches approximately at  $\sim 2.34 \times 10^6$  cells for a circular cell monolayer of 25 mm diameter, we prepare the coverslip with a circular cell monolayer for rheological experiments.

### III. RESULTS

We start our study of the material properties of cell monolayer by applying sinusoidal strain oscillations. For viscoelastic materials in the linear regime, we have

$$\begin{aligned} \gamma(\omega t) &= \gamma_0 \sin(\omega t), & (1) \\ \sigma(\omega t) &= G' \gamma_0 \sin(\omega t) + G'' \gamma_0 \cos(\omega t), & (2) \\ \tan(\delta) &= \frac{G''}{G'}, & (3) \end{aligned}$$

where  $\omega$  is the angular frequency of the oscillatory shear  $\gamma(\omega t)$ ,  $t$  is the time,  $\gamma_0$  is the amplitude of the oscillatory shear,  $\sigma(\omega t)$  is the stress,  $G'$  is the storage modulus,  $G''$  is the loss modulus, and  $\delta$  is the loss tangent. For the non-linear regime, the stress response can be expressed as a Fourier series,<sup>39</sup>

$$\sigma(\omega t) = \sum_{n, odd} \sigma_n(\omega, \gamma_0) \sin(n\omega t + \delta_n(\omega, \gamma_0)), \quad (4)$$

where  $\sigma_n(\omega, \gamma_0)$  are stress amplitudes and  $\delta_n(\omega, \gamma_0)$  are phases for all harmonics “ $n$ .” In the linear viscoelastic (LV) regime, the stress response will include only the first harmonic,  $n = 1$ , whereas nonlinearity at higher shear strains results in the growth of higher harmonic contributions.<sup>40,41</sup> We aim to explore the linear and non-linear response of the epithelial cell monolayer. In this work, we adopted the same notation and definition of parameters ( $G'_M, G'_L$  and  $G''_M, G''_L$ ) as in Ewoldt *et al.*<sup>40</sup> and Argatov *et al.*<sup>42</sup>

In all our experiments, the total gap between the rheometer plates is the sum of the thickness of the glass coverslip 150–190  $\mu\text{m}$  and the cell monolayer  $\sim 7 \mu\text{m}$ , which is ranging from  $\sim 160$  to 200  $\mu\text{m}$ . The bottom glass plate is used to set the zero for the rheometer before starting the experiments. After that, we fix the glass coverslip with a circular cell monolayer [Fig. 2(b)] on the bottom glass plate as shown in Figs. 2(c) and 2(d). The “dimensionless relative shear strain” on the cell monolayer will now be estimated by scaling the shear strain readings from the instrument,  $\gamma\%$ , by initial  $\gamma_0$ . We scaled the shear strain  $\gamma\%$  as

$$\hat{\gamma} = \frac{\gamma}{\gamma_0}. \quad (5)$$

#### A. Oscillatory amplitude sweep

For the oscillatory amplitude sweep experiments, the shear strain ( $\gamma$ ) was applied from 0.01% to 100% (and 10% for LAOS), which corresponds to dimensionless relative shear strain  $\hat{\gamma}$  from 1 to 10 000 (and 1000 for LAOS) at a frequency of  $\omega = 5 \text{ rad/s}$  on the cell monolayer for both cases: (a) without serum (FBS = 0%) and (b) with serum (FBS = 10%). Figure 5 shows the first-order (linear) storage modulus ( $G'$ ) and loss modulus ( $G''$ ) along with the non-linear viscoelastic (NLV) moduli:  $G'_M$  is the storage/elastic modulus at minimum strain,  $G'_L$  is the storage/elastic modulus at large strain and similarly  $G''_M$  is the loss/viscous modulus at minimum strain,  $G''_L$  is the loss/viscous

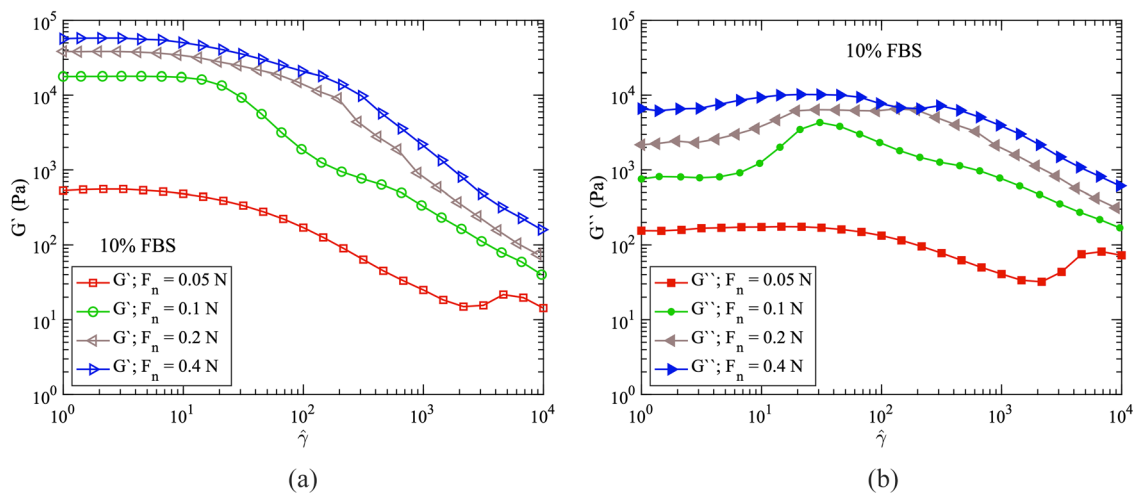
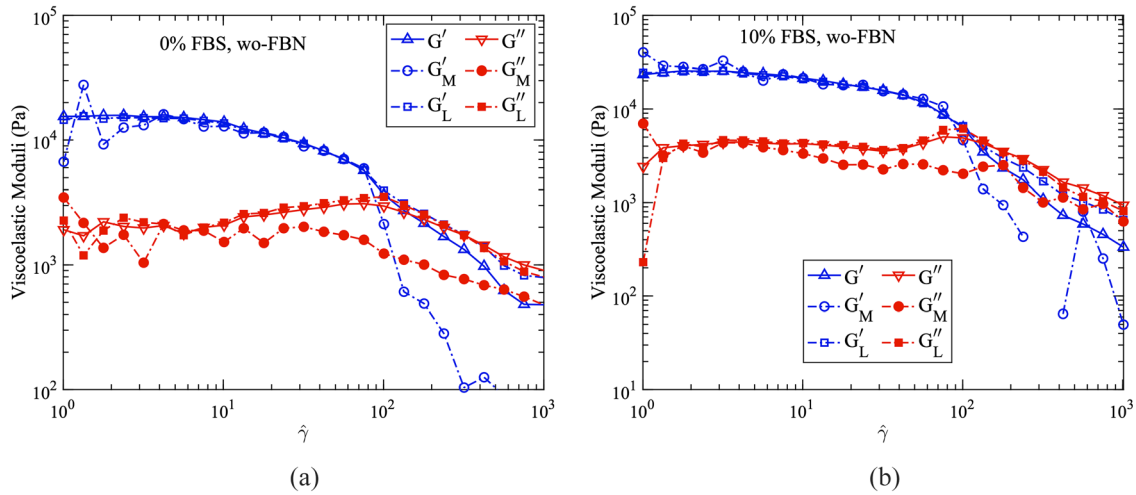


FIG. 4. Amplitude Sweep with increasing normal force. The (a) storage modulus  $G'$  and (b) the loss modulus  $G''$  for cell monolayer with 10% FBS for a different normal force.



**FIG. 5.** Amplitude sweep of the cell monolayer at a frequency of 5 rad/s. The viscoelastic moduli ( $G'_M, G'_L$  and  $G''_M, G''_L$ ) of monolayer with (a) 0% FBS; (b) 10% FBS concentration as a function of dimensionless relative shear strain ( $\hat{\gamma}$ ).

modulus at large strain, as the function of dimensionless relative shear strain  $\hat{\gamma}$  for serum-starved (FBS = 0%) and healthy (FBS = 10%) cell monolayers. For both cases, the value of linear viscoelastic moduli ( $G'$  and  $G''$ ) and non-linear viscoelastic moduli ( $G'_L$  and  $G''_L$ ) remains constant up to  $\hat{\gamma} \sim 8$  and then decreases with the increase in  $\hat{\gamma}$  (Fig. 5). For low deformation up to  $\hat{\gamma} \leq 8$  where storage modulus  $G'$  is independent of  $\hat{\gamma}$  is called *linear viscoelastic* (LV) region and *nonlinear viscoelastic* (NLV) region after  $\hat{\gamma} > 8$ . The viscoelastic moduli are slightly higher for healthy cell monolayer with 10% FBS [Fig. 5(b)] than serum-starved cell monolayer at 0% FBS [Fig. 5(a)].

After the constant range up to  $\hat{\gamma} \sim 8$ , the storage modulus  $G'$  decays with a higher rate as compared to the loss modulus  $G''$ , and a tipping or crossover point occurs after which  $G''$  become higher than  $G'$ . Before the crossover point, the cell monolayer behaves like an elastic solid (storage modulus dominates over loss modulus). However, after the crossover point, it becomes like a viscous fluid (loss modulus dominates over storage modulus). The transition from elastic solid-like to viscous fluid-like behavior is observed at a sufficiently high value of strain ( $\hat{\gamma} > 10^2$ ) because the cell monolayer may be stretching without significant cell cytoskeleton remodeling (biopolymer network in the cell) for the small strain values. However, with the increase in strain values, there may be a significant restructuring of the cytoskeleton in the cells (biopolymer network in the cells start breaking), resulting in decreased storage and loss moduli. This can be attributed to the fact that biopolymer linking has distributed strength. First, the links with the smallest strength start breaking, resulting in reducing the monolayer's rheological properties. We also observe that the nonlinear viscoelastic moduli ( $G'_M$  and  $G''_L$ ) deviate from the linear viscoelastic moduli,  $G'$  and  $G''$  at much higher dimensionless relative shear strain ( $\hat{\gamma}$ ) for both serum-starved and healthy cell monolayers.

Furthermore, as shown in Fig. 5, the storage and loss moduli show power-law dependence on the applied strain after the crossover. The rate of reduction of the value of the storage modulus is more than the loss modulus for both cell monolayer cases with and without serum (Fig. 5), as some of the broken contacts of biopolymers may

help in maintaining the frictional losses. Hence, the loss modulus starts dominating over the storage modulus after a particular strain value.

For complex materials, the crossover of the storage and loss moduli is also a function of applied oscillatory shear strain frequency. We investigated this effect of the frequency on the crossover by conducting experiments at  $\omega = 1$  and 10 rad/s. As shown in Fig. 6, the crossover has delayed for both healthy (10% FBS) and serum-starved (0% FBS) cell monolayer for  $\omega = 10$  rad/s. This delay is more noticeable for the serum-starved cell monolayer at 0% FBS. For the healthy cell monolayer at 10% FBS, the storage modulus  $G'$  and the loss modulus  $G''$  are lower at high frequency  $\omega = 10$  rad/s and the crossover is also earlier, as compared to the cell monolayer with no-serum (0% FBS), where the moduli ( $G'$  and  $G''$ ) are higher and delayed crossover was observed at high frequency.

Further insight into the material behavior can be investigated by plotting the normalized storage modulus [ $\hat{G}' = G'/G'(0)$ ] and the normalized loss modulus [ $\hat{G}'' = G''/G''(0)$ ] as a function of applied strain.<sup>43,44</sup> As seen in Fig. 7, the cell monolayer shows a pronounced local maximum in the loss modulus ( $\hat{G}''$ ). This type of behavior is called as *weak strain overshoot* and is the signature behavior of soft glassy materials.<sup>43,44</sup> Hyun *et al.*<sup>44</sup> and Sim *et al.*<sup>45</sup> explained the possible mechanism using a network model composed of segments and junctions. A *segment* is defined as a part of a macromolecular chain or a microstructure joining two successive junctions. The *junctions* are defined as the points where the intra- or intermolecular interactions are localized and may be regarded as the cross-linking points. The segments are created and lost during the flow, and their creations and loss rates give the distribution of junctions.

The weak strain overshoot behavior results from positive creation and loss parameters, with a creation parameter smaller than the loss parameter. With this range of parameters, the creation and the loss terms increase with the strain amplitude, and the destruction rate grows faster than that of creation. The positive creation parameter accounts for the increased connectivity of the network (or other microstructure arising from interactions). It initially leads to the

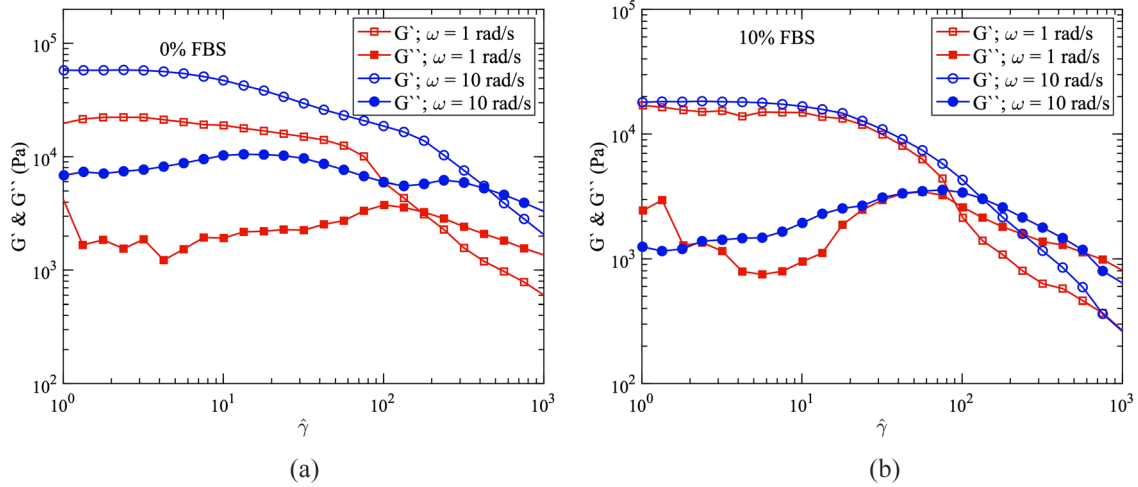


**FIG. 6.** Amplitude sweep of the cell monolayer at a frequency of  $\omega = 1$  and 10 rad/s and without (woFBN) fibronectin coating. The shear moduli ( $G'$  and  $G''$ ) of monolayer with (a) 0% FBS; (b) 10% FBS concentration as a function of dimensionless relative shear strain ( $\dot{\gamma}$ ).

increased dissipation, while the loss term becomes dominant at higher strains, which results in an overall decrease in both the storage ( $\hat{G}'$ ) and loss ( $\hat{G}''$ ) moduli. The local maximum of the loss modulus  $\hat{G}''$  may be the result of the balance between the formation and the destruction of the network junctions.

The strain overshoot behavior in the loss modulus  $\hat{G}''$  highly depends on the class of soft material. For the cell monolayer, the increase in  $\hat{G}''$  may be partly related to the destruction of the microstructures developed during the imposed oscillatory shear strain, and the reformation process of the microstructures may cause the overshoot behavior. The local maximum in loss modulus is more pronounced for the healthy cell monolayer with 10% FBS [Fig. 7(b)] than for the starved cell monolayer [Fig. 7(a)], again confirming that in the absence of the serum, the cell monolayer loses the ability to restructure itself.

This can also be seen in the graph of  $\tan(\delta) = G''/G'$  in Fig. 8. After the crossover point, the values of  $\tan(\delta)$  become more than unity and continue to increase afterward (Fig. 8). The values of  $\tan(\delta)$  for serum-starved (0% FBS) cell monolayer are higher than that of healthy (10% FBS) cell monolayer throughout the range of applied strain. Healthy cells have a dynamic cytoskeleton with different kinds of protein fibers such as actin, myosin, microtubules, and intermediate filaments, which give rigidity and structure to the cells. In the absence of the serum, cells lack the proteins and other nutrients to form the dynamic filaments, thus reducing the load-bearing capacity and the restructuring capabilities of the cells and the monolayer, which results in the more fluidic nature of the starved cell monolayer at larger strain values, which results in higher ratios of loss to storage modulus (or  $\tan \delta$ ) for starving cell monolayer (with 0% FBS), than that for healthy cell monolayer (with 10% FBS).

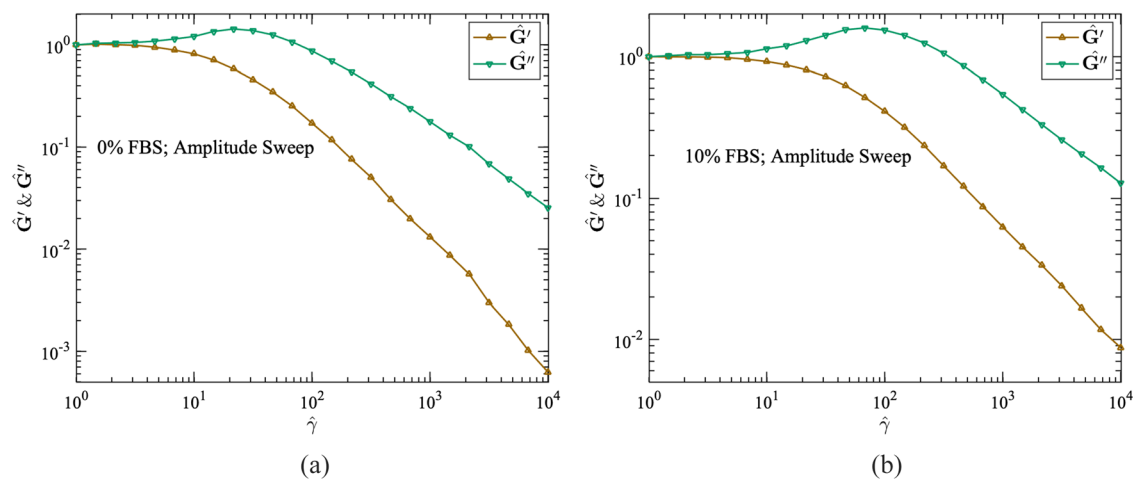


**FIG. 7.** Amplitude sweep of the cell monolayer at a frequency of  $\omega = 5$  rad/s. The normalized shear moduli ( $\hat{G}'$  and  $\hat{G}''$ ) for monolayer with (a) 0% FBS; (b) 10% FBS concentration as a function of dimensionless relative shear strain ( $\dot{\gamma}$ ).

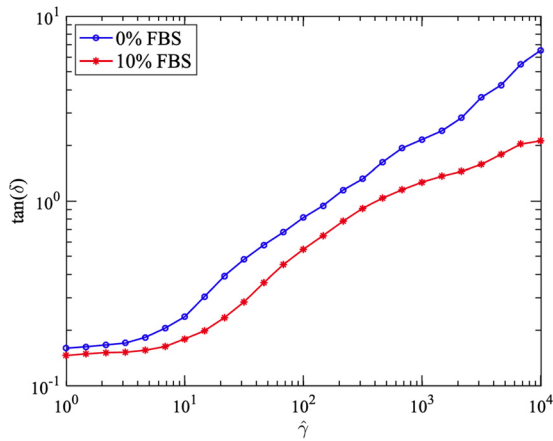


FIG. 8. The value of  $\tan(\delta) = G''/G'$  vs dimensionless relative shear strain ( $\hat{\gamma}$ ), at 0% and 10% FBS concentration.

1. LAOS experiments

Since the cell monolayer is mostly shearing in the non-linear region at high values of strain, we have conducted large amplitude oscillatory shear (LAOS) experiments to understand its behavior in the non-linear region. We have used the MITlaos software (version 2.2 for Beta for Matlab) developed by Ewoldt *et al.*<sup>40</sup> as well as the raw data from the rheometer software (RheoCompass) to analyze the LAOS data. Following Kamkar *et al.*,<sup>46</sup> we also control the wall-slip by coating the upper plate with fibronectin, which acts as a glue between the surface and the cell monolayer. Since the cells have already adhered to the bottom glass coverslip, fibronectin provides the attachment between the cell monolayer and the upper plate. Thus, the cell monolayer is now attached with both upper and lower plates. We conducted the LAOS experiments with (a) the upper plate coated with Fibronectin (wFBN) and (b) without

Fibronectin coating on the upper plate (woFBN). Figure 9 shows the effect of Fibronectin for both cases (a) without serum (FBS = 0%) and (b) with serum (FBS = 10%).

Even though the qualitative behavior is the same for the serum-free (0% FBS) and healthy (10% FBS) cell monolayer for with and without fibronectin-coated upper plate, the effect of adhesion due to Fibronectin is more pronounced for serum-free (0% FBS) cell monolayer. The storage modulus  $G'$  is significantly higher throughout the full range of  $\hat{\gamma}$  when the cell monolayer is attached with upper plate using fibronectin (wFBN) than that of when there is no fibronectin (woFBN) as shown in Fig. 9(a), whereas for the healthy cell monolayer at 10% FBS, there is no significant difference in storage modulus  $G'$  at lower strains ( $\hat{\gamma} \leq 60$ ). At higher strains,  $\hat{\gamma} > 60$ , the storage modulus  $G'$  is higher for fibronectin-coated plate (wFBN) than that of without fibronectin (woFBN) as shown in Fig. 9(b).

For both conditions of the cell monolayer (a) without serum (FBS = 0%) and (b) with serum (FBS = 10%), the crossover is delayed up to  $\hat{\gamma} = 600 - 700$  when the cell monolayer is glued to the upper plate using fibronectin (wFBN). The cell monolayer's behavior as shown in Fig. 9 suggests that for a healthy cell monolayer at 10% FBS, the effect of Fibronectin was not significant. Only at higher strain values, the adhesion effect becomes more important for healthy monolayer [Fig. 9(b)], whereas the serum-free cell monolayer experiences the effect of fibronectin adhesion even at lower strains [Fig. 9(a)].

Following Hyun *et al.*<sup>43,44</sup> and Kamkar *et al.*,<sup>46</sup> we plotted the normalized storage modulus [ $\hat{G}' = G'/G'(0)$ ] and the normalized loss modulus [ $\hat{G}'' = G''/G''(0)$ ] as a function of applied dimensionless relative shear strain ( $\hat{\gamma}$ ) for LAOS experiments (Fig. 10). The effect of adhesion on the cell monolayer for the fibronectin-coated upper plate (wFBN) is more pronounced for serum-starved condition [Fig. 10(a)]. The qualitative behavior of serum-free and healthy cell monolayer for with (wFBN) and without (woFBN) fibronectin-coated upper plate remains similar, i.e., Type III,<sup>43,44</sup> which is expected as the cytoskeleton's long biopolymer fibers dynamically change (assemble and disassemble) as per the applied strain.

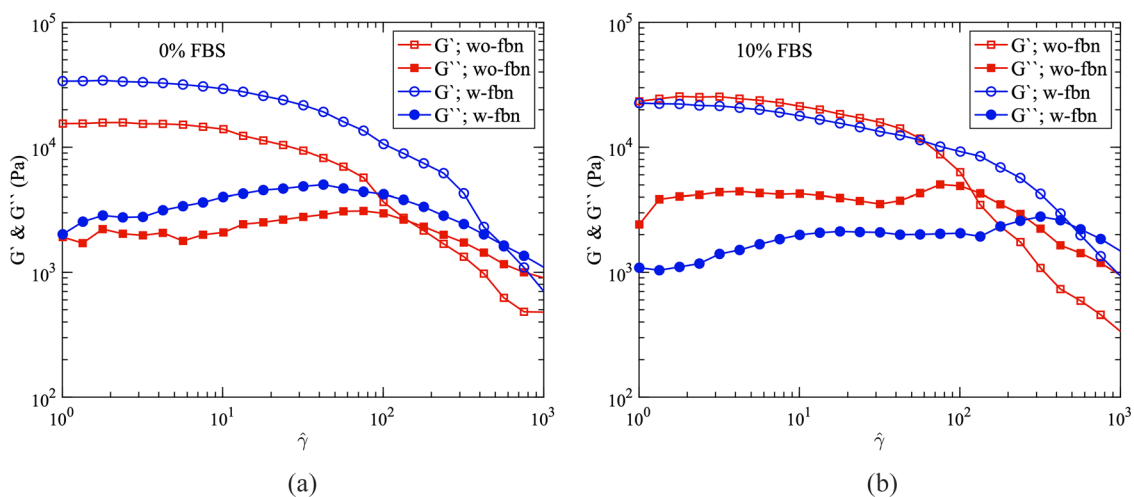
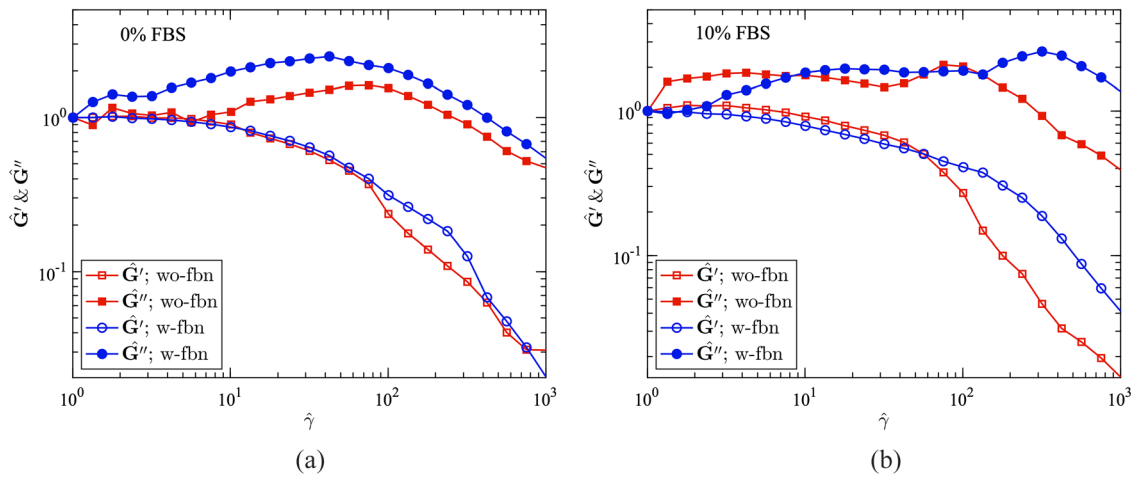


FIG. 9. Amplitude sweep of the cell monolayer at a frequency of 5 rad/s and with (wFBN) and without (woFBN) fibronectin coating. The shear moduli ( $G'$  and  $G''$ ) of monolayer with (a) 0% FBS; (b) 10% FBS concentration as a function of dimensionless relative shear strain ( $\hat{\gamma}$ ).



**FIG. 10.** Amplitude sweep of the cell monolayer at a frequency of 5 rad/s and with (wFBN) and without (woFBN) fibronectin coating. The normalized shear moduli ( $\hat{G}'$  and  $\hat{G}''$ ) for monolayer with (a) 0% FBS; (b) 10% FBS concentration as a function of dimensionless relative shear strain ( $\hat{\gamma}$ ).

*a. Lissajous–Bowditch curves.* The LAOS data are mostly represented as Lissajous–Bowditch curves, which represent the dependence of shear stress on applied shear strain (or rate of strain).<sup>40,41,47,48</sup> Here we report the data of LAOS experiments done with the cell monolayer at 0% FBS and 10% and with fibronectin-coated upper plate (wFBN) and without fibronectin coating on the upper plate (woFBN) at frequency  $\omega = 5$  rad/s and at a dimensionless relative shear strain amplitude range of  $\hat{\gamma} = [1 - 1000]$ . Figure 11 shows the elastic Lissajous–Bowditch curves. The individual orbit is centered at (wFBN/woFBN,  $\hat{\gamma}$ ) to give an overview of the cell monolayer’s response over a range of dimensionless relative shear strain  $\hat{\gamma}$  and with and without fibronectin coating on the upper plate for both cases (a) 0% FBS [Fig. 11(a)] and (b) 10% FBS [Fig. 11(b)]. The symmetric elliptic curves indicate the linear viscoelastic region with two mirror planes and the non-linear region by the asymmetric elliptic curve. Figure 11 shows that even at low dimensionless relative shear strain  $\hat{\gamma}$ , the elastic Lissajous–Bowditch curves are slightly different for with (wFBN) and without (woFBN) fibronectin-coated upper plate for both healthy (10% FBS) and starved (0% FBS) cell monolayers. The onset of non-linearity is much earlier in the case of without fibronectin (woFBN) coated upper plate, whereas the cell monolayer with 0% and 10% FBS, which is attached to the upper plate using fibronectin coating (wFBN), shows the much-delayed onset of non-linearity.

**B. Frequency sweep**

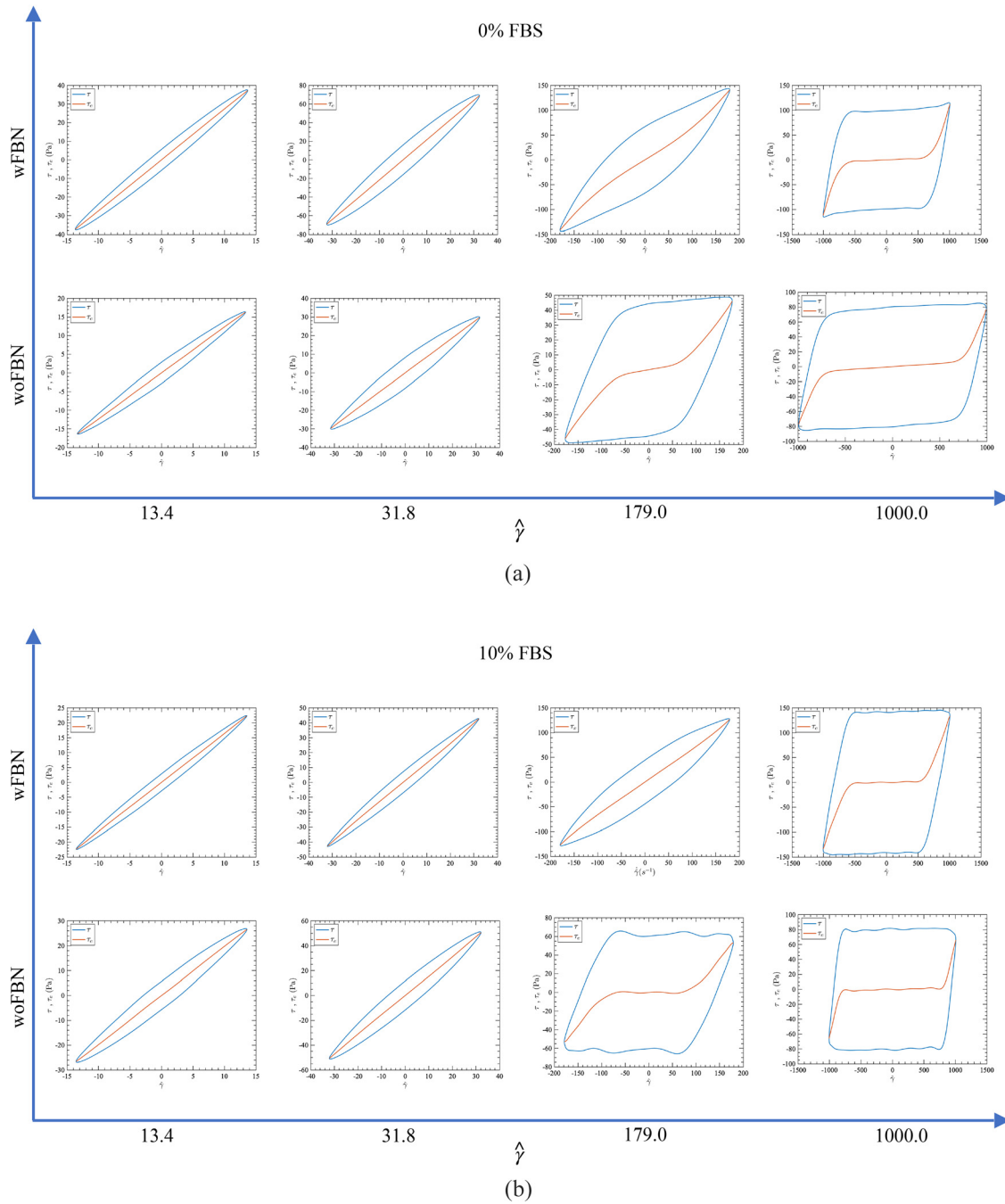
The frequency sweep experimental data are shown in Figs. 12–15 for 0% and 10% FBS. We have applied the frequency sweep in the linear and non-linear viscoelastic regime for both cases. We apply the frequency of  $\omega = 100$  to 1 rad/s at a dimensionless relative shear strain of  $\hat{\gamma} = 5$  in linear regime [Figs. 12(a) and 12(b)] and  $\hat{\gamma} = 500$  [Figs. 13(a) and 13(b)] and 5000 [Figs. 14(a) and 14(b)] in non-linear regime for 0% and 10% FBS. The values of both  $G'$  and  $G''$  are decreasing as we increase the dimensionless relative shear strain from  $\hat{\gamma} = 5$  to  $\hat{\gamma} = 500$  and  $\hat{\gamma} = 5000$ . In the linear regime at  $\hat{\gamma} = 5$ , the storage modulus  $G'$  is higher than the loss modulus  $G''$  throughout the whole frequency range from  $\omega = 100$  to 1 rad/s, whereas in the non-linear regime at

$\hat{\gamma} = 500$  and  $\hat{\gamma} = 5000$ , the  $G'$  is lower than  $G''$ , which shows the fluid-like behavior of the cell monolayer in the nonlinear regime.

The cell monolayer without serum shows the weak power-law dependence of the storage modulus,  $G'$  and loss modulus,  $G''$  with an exponent of “ $s \approx 0.15$ ” and “ $s \approx 0.14$ ” in the linear viscoelastic regime with  $\hat{\gamma} = 5$  throughout the frequency range [Fig. 12(a)], respectively. However, in the non-linear regime, we observed the stronger dependence of storage and loss moduli at higher frequencies. For  $\hat{\gamma} = 500$ , the power-law exponent is “ $s = 0.12$ ” and “ $s = 0.13$ ” for  $G'$  and  $G''$  at low frequencies ( $\omega \leq 20$  rad/s), respectively. Both  $G'$  and  $G''$  show stronger dependence on the frequency at higher frequencies ( $\omega \geq 30$  rad/s). However,  $G'$  shows stronger dependence on the frequency with the power-law exponent of “ $s = 0.42$ ,” while the loss modulus  $G''$  is having exponent of “ $s = 0.26$ ” [Fig. 13(a)]. Figure 14(a) shows that both moduli at even higher dimensionless relative shear strain ( $\hat{\gamma} = 5000$ ) show stronger dependence on frequencies than lower dimensionless relative shear strains ( $\hat{\gamma} = 5$  and  $\hat{\gamma} = 500$ ). At low frequencies below  $\omega \leq 20$  rad/s,  $G'$  and  $G''$  are having power-law exponent of “ $s = 0.27$ ” and “ $s = 0.26$ ,” respectively. At higher frequencies  $\omega \geq 30$  rad/s,  $G'$  shows more dependence than  $G''$  with power-law exponents of “ $s = 0.82$ ” and “ $s = 0.63$ ,” respectively.

For full serum case (10% FBS), the storage modulus  $G'$  and the loss modulus  $G''$  show a weak dependence on frequency in the linear and nonlinear viscoelastic regime throughout the range of applied frequencies. In linear viscoelastic regime at  $\hat{\gamma} = 5$ , [Fig. 12(b)] the loss modulus  $G''$  shows a stronger dependence at high frequencies ( $\omega \geq 20$  rad/s) with a power-law exponent of “ $s = 0.27$ .” However, at lower frequencies ( $\omega \leq 20$  rad/s),  $G''$  shows weak power-law dependence with an exponent of “ $s = 0.12$ ,” whereas the storage modulus  $G'$  shows the weaker power-law dependence throughout the applied frequency range with an exponent of “ $s = 0.13$ .” In the non-linear viscoelastic regime, at  $\hat{\gamma} = 500$  [Fig. 13(b)], the loss modulus shows similar behavior in the linear regime, but with lower values. The power-law dependence is weaker at lower frequencies with an exponent of “ $s = 0.12$ ” and stronger with an exponent of “ $s = 0.46$ ” at higher frequencies. The storage modulus  $G'$  also shows the weak dependence

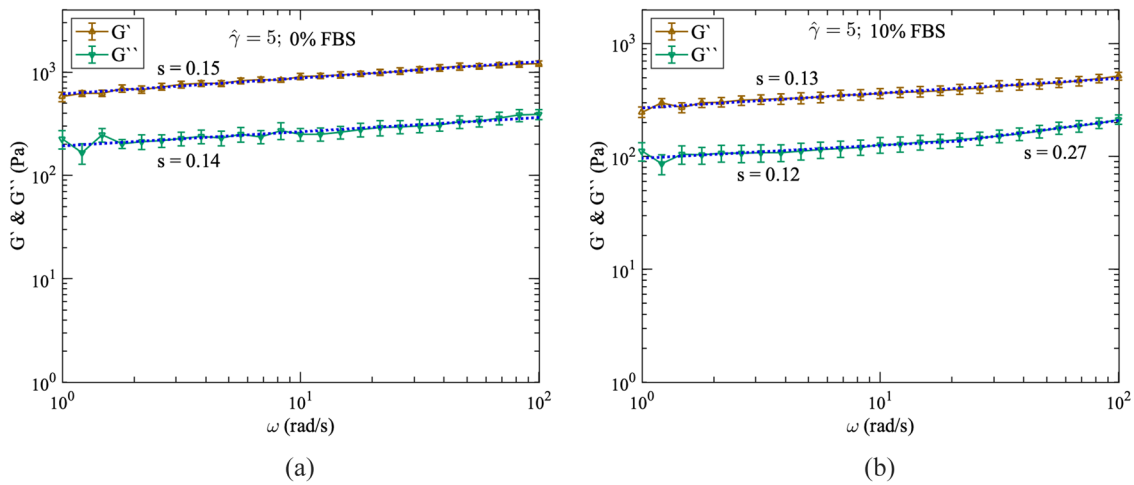
04 December 2023 12:00:51



**FIG. 11.** Elastic Lissajous–Bowditch curves for the cell monolayer at a frequency of 5 rad/s and with (wFBN) and without (woFBN) fibronectin coating and for monolayer with (a) 0% FBS; (b) 10% FBS concentration as a function of dimensionless relative shear strain ( $\dot{\gamma}$ ).

with much lower values but with the same power-law exponent of “ $s = 0.08$ .” The loss modulus is higher than the storage modulus, indicating the fluidic nature of the material. At even higher dimensionless relative shear strain amplitude at  $\dot{\gamma} = 5000$  [Fig. 14(b)] in the nonlinear regime, the storage and loss moduli show weak dependence on

frequencies throughout the applied range, except for loss modulus, which shows the power-law dependence with an exponent of “ $s = 0.57$ ” at very high frequencies. The storage modulus values are slightly higher at low frequencies ( $\omega \leq 20$ ) and lower at high frequencies ( $\omega \geq 20$ ), but the exponent of power-law is “ $s = -0.09$ .”



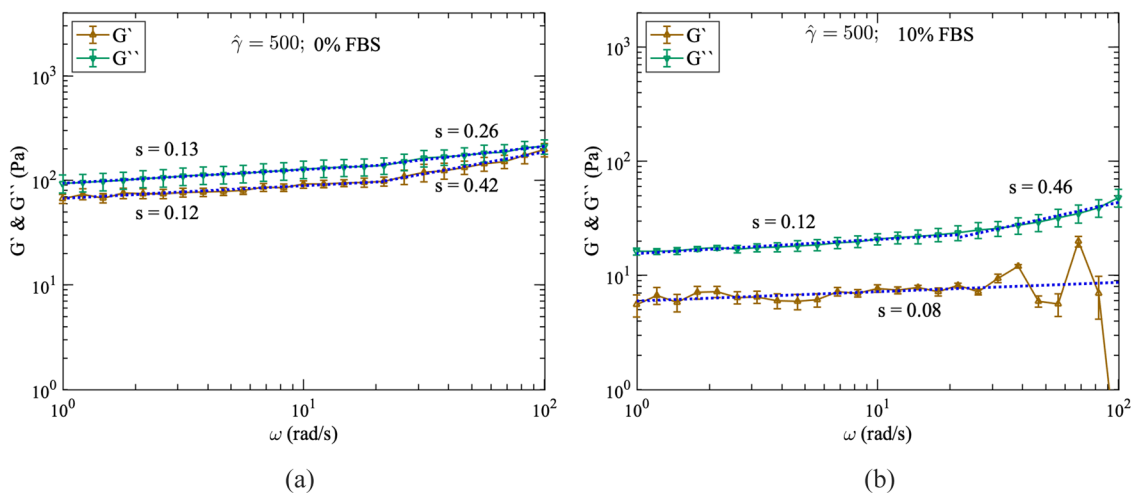
**FIG. 12.** Frequency sweep of the cell monolayer at a constant dimensionless relative shear strain amplitude,  $\hat{\gamma} = 5$ . The shear moduli ( $G'$  and  $G''$ ) of the monolayer with (a) 0% FBS and (b) 10% FBS concentration as a function of frequency,  $\omega$  (rad/s). The power law exponent is shown as “s” for different plots.

Figure 15(a) shows the variation of  $\tan(\delta) = G''/G'$  with frequency for  $\hat{\gamma} = 5, 500$ , and 5000 for starved cell monolayer at 0% FBS. In the linear viscoelastic regime at  $\hat{\gamma} = 5$ ,  $\tan(\delta)$  is lowest and does not show dependence with the frequency throughout the applied frequency range  $\omega = 100$  to 1 rad/s. Also, in the nonlinear regime,  $\tan(\delta)$  does not depend on applied frequency, but the values are close to 1 and 10 for  $\hat{\gamma} = 500$  and 5000, respectively. This may be attributed to the fluidic nature of starved cell monolayer at large deformations.

The ratio of loss modulus and storage modulus,  $\tan \delta$  is shown in Fig. 15(b) for a healthy cell monolayer with 10% FBS. Similar to the starved cell monolayer at 0% FBS, the  $\tan \delta$  in the linear viscoelastic regime at  $\hat{\gamma} = 5$  does not depend on the applied frequency. Similar behavior can be seen for higher deformation at  $\hat{\gamma} = 500$  and 5000. The values of  $\tan \delta$  for  $\hat{\gamma} = 5$  are lowest compared to  $\hat{\gamma} = 500$  and 5000.

However, in the case of healthy cell monolayer, the values of  $\tan \delta$  for  $\hat{\gamma} = 500$  and 5000 are much closer, i.e., approximately 4 [Fig. 15(b)], whereas, for the starved cell monolayer, the values of  $\tan \delta$  for  $\hat{\gamma} = 500$  and 5000 are close to 1 and 10 [Fig. 15(a)], respectively. This difference between starved cell monolayer at 0% FBS and healthy cell monolayer at 10% FBS is due to the presence of serum, which provides the necessary nutrients and proteins to the cells for restructuring the cytoskeleton inside the cells and the contacts with other cells in the cell monolayer. In the absence of the serum, a cell cannot form necessary proteins and contacts, thus becoming more fluidic at large deformations.

Serum-starved cell monolayer shows a strong power-law dependency at a large dimensionless relative shear strain amplitude value ( $\hat{\gamma} = 5000$ ) and higher frequency values [Fig. 14(a)]. This indicates



**FIG. 13.** Frequency sweep of the cell monolayer at a constant dimensionless relative shear strain amplitude,  $\hat{\gamma} = 500$ . The shear moduli ( $G'$  and  $G''$ ) of the monolayer with (a) 0% FBS and (b) 10% FBS concentration as a function of frequency,  $\omega$  (rad/s). The power law exponent is shown as “s” for different plots.

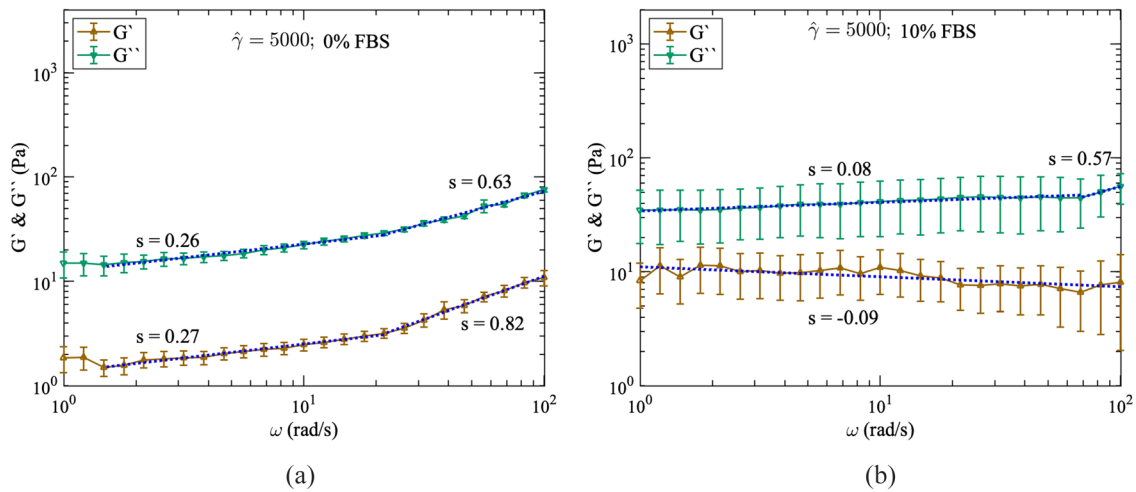


**FIG. 14.** Frequency sweep of the cell monolayer at a constant dimensionless relative shear strain amplitude,  $\hat{\gamma} = 5000$ . The shear moduli ( $G'$  and  $G''$ ) of the monolayer with (a) 0% FBS and (b) 10% FBS concentration as a function of frequency,  $\omega$  (rad/s). The power law exponent is shown as “s” for different plots.

that the serum-starved cell monolayer becomes stiff at large values of dimensionless relative shear strain amplitude at high frequency, whereas the cell monolayer with FBS 10% remains flexible even at high values of  $\hat{\gamma}$  and  $\omega$ , as a power-law dependency remains weak for the cell monolayer with 10% FBS.

We attribute these differences between starved cell monolayer at 0% FBS and healthy cell monolayer at 10% FBS to the presence of serum, which provides the necessary nutrients and proteins to the cells for restructuring the cytoskeleton inside the cells and the contacts with other cells in the cell monolayer. In the absence of the serum, a cell cannot form necessary proteins and contacts, thus becoming more fluidic at large deformations. Furthermore, a detailed non-linear analysis of frequency sweep is needed to fully understand the behavior of cell monolayer for high shear strains. In this work, we present a simplistic

approach to access the effect of serum starvation on the cell monolayer.

### C. Oscillatory step strain experiments

Next, we applied a step-change in the amplitude of the oscillatory shear strain to the cell monolayer to probe more into the bulk rheology of the cell monolayer. Here, we start by applying a dimensionless relative shear strain amplitude of  $\hat{\gamma} = 2$  for 60 s, apply a step increase in  $\hat{\gamma} = 8$  for next 300 s, and then decrease  $\hat{\gamma}$  to the initial value of  $\hat{\gamma} = 2$  for next 600 s. For another step, we apply  $\hat{\gamma} = 500$  for 300 s after the initial  $\hat{\gamma} = 2$  and then decrease the dimensionless relative shear strain amplitude to the initial value of  $\hat{\gamma} = 2$  for next 600 s. This procedure is repeated for both cases: (1) serum-free (0% FBS) and (2) with serum (10% FBS).

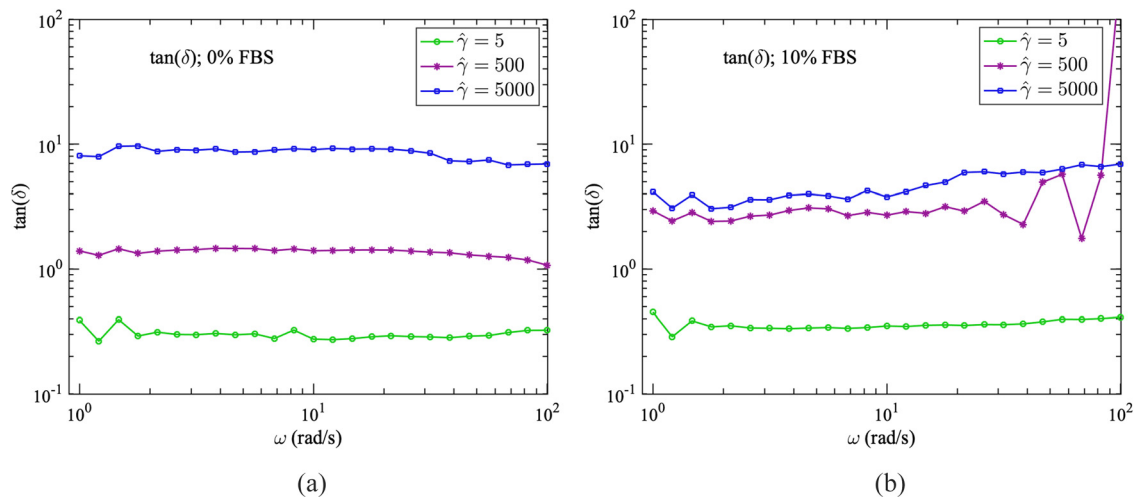


**FIG. 15.** Frequency sweep of the cell monolayer at a constant dimensionless relative shear strain amplitude. The  $\tan(\delta) = G''/G'$  of the monolayer with (a) 0% FBS and (b) 10% FBS concentration as a function of frequency,  $\omega$  (rad/s).

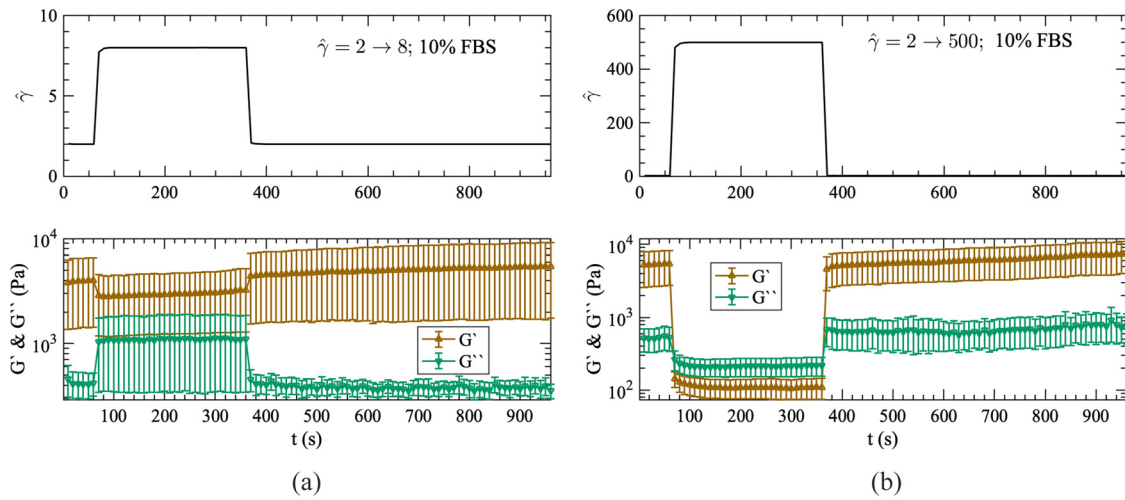


FIG. 16. Step increase in dimensionless relative shear strain amplitude: (a)  $\hat{\gamma} = 2 \rightarrow 8$  and (b)  $\hat{\gamma} = 2 \rightarrow 500$  for 10% FBS.

Healthy cells, with 10% FBS, completely recover small deformation immediately as shown in Fig. 16(a), confirming elastic behavior of healthy monolayer cells for small deformations ( $\hat{\gamma} = 2-8$ ). In the non-linear viscoelastic regime ( $\hat{\gamma} = 2-500$ ) as shown in Fig. 16(b), we see almost full recovery with a small time lag. This may happen as the cell monolayer is deformed beyond the elastic limit, and deformation may reach a viscoplastic regime where the loss modulus  $G''$  is larger than the storage modulus  $G'$ . In this large deformation limit, some links of cytoskeleton biopolymers might be broken permanently. However, after a long time, it is expected to regain the broken links, and the material properties should return to the original value. Further confirming that healthy cell monolayers are flexible and capable of instant complete recovery of the material properties in the case of small deformation/strain and delayed recovery in large deformation [Fig. 18(b)], whereas serum-free cell monolayer at 0% FBS does not show complete

recovery even at a small value of dimensionless relative shear strain amplitude ( $\hat{\gamma} = 2-8$ ) as shown in Fig. 17(a), indicating the inability of starved cell monolayer for reconciliation in cell structure and cell monolayer morphology. The slip at upper plate may also be playing some role, which needs to be further investigated in future studies.

The step-change in dimensionless relative shear strain amplitude of higher value ( $\hat{\gamma} = 2-500$ ) alters the rheological properties of the serum-starved cell monolayer [Fig. 17(b)]. The cell monolayer does not show full recovery at 0% FBS [Fig. 18(a)]. This may happen as the cross-linking of the biomolecules inside the cells and at the cell-cell junction in the cell monolayer is once broken, it will be unable to rebuild these crosslinks due to lack of serum. Hence, the rheological properties of starved cell monolayer at 0% FBS after deformation reduce permanently.

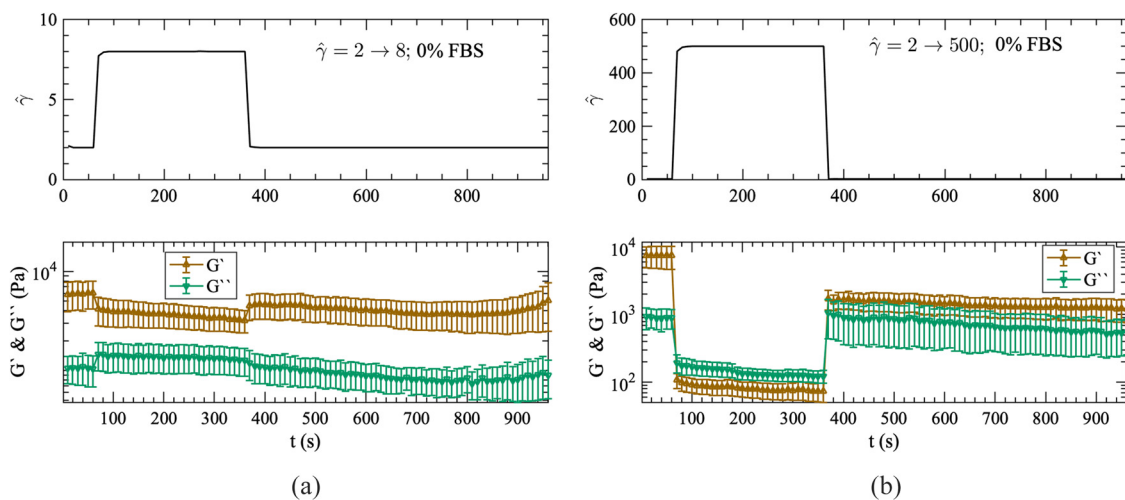


FIG. 17. Step increase in dimensionless relative shear strain amplitude: (a)  $\hat{\gamma} = 2-8$  and (b)  $\hat{\gamma} = 2-500$  for 0% FBS.

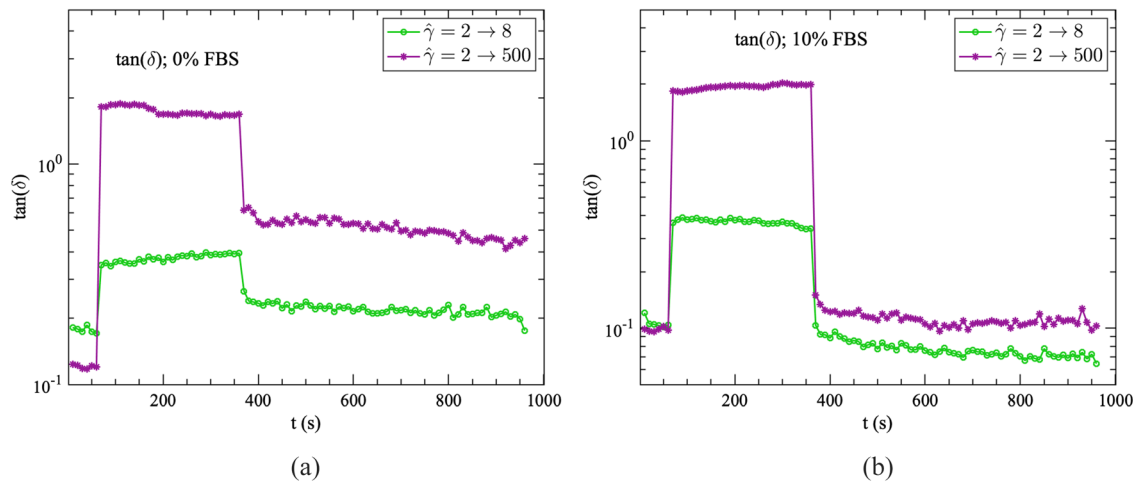


FIG. 18. Comparison of  $\tan \delta$  for the step increase in dimensionless relative shear strain amplitude for the monolayer with (a) 0% FBS and (b) 10% FBS.

In Fig. 19, the values of stress  $\sigma$  are shown for the step-change in dimensionless relative shear strain amplitude experiments. For small deformations ( $\hat{\gamma} = 2-8$ ) as shown in Fig. 19(a), the stress for a starved cell monolayer increases instantly as the step deformation is applied and then decreases, whereas the stress in a healthy cell monolayer increases with the step-change in  $\hat{\gamma}$ , but remains much lower than that of the starved cell monolayer, and then smoothly increases during the applied  $\hat{\gamma}$ . At the end of the step-change in  $\hat{\gamma}$ , the values of the stress in cell monolayer with and without serum become equal. As the step-change in dimensionless relative shear strain amplitude is removed, the stress in healthy cell monolayer returns to initial stress before the step-change in  $\hat{\gamma}$  and remains constant with time, but the stress in the starved cell monolayer shows some variations with time after the step-change in dimensionless relative shear strain amplitude is removed. This observation shows that a healthy cell monolayer can effectively distribute

the stress due to small deformation and prevent the stresses from increasing abruptly in the cell monolayer. This may be because of the many dynamic protein filaments in the cell cytoskeleton responsible for rigidity and restructuring of the cells, redistributing the stress effectively in the cytoskeleton and throughout the cell monolayer, whereas, in the starving cell monolayer, the cell cytoskeleton may not form these fibrous proteins and thus unable to distribute the stress effectively.

For large deformations ( $\hat{\gamma} = 2-500$ ), as shown in Fig. 19(b), the stress in a healthy cell monolayer is three times higher than for a starved cell monolayer. The stress returns to its initial value after the step-change in dimensionless relative shear strain amplitude for cell monolayer with and without serum. The starved cell monolayer shows a slight decrease in stress with time after the step change in dimensionless relative shear strain amplitude, whereas the stress remains constant in the healthy cell monolayer.

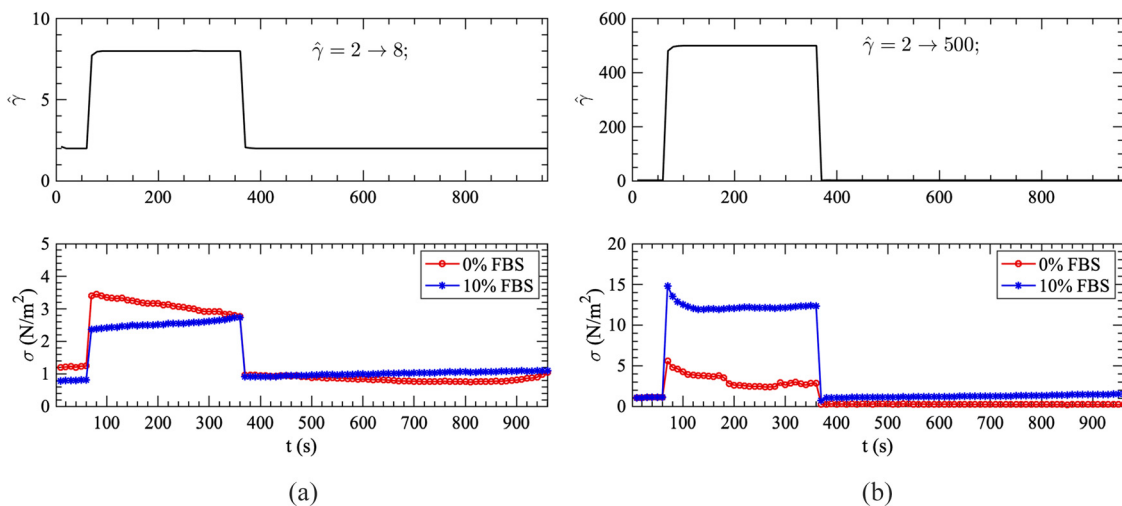


FIG. 19. Comparison of  $\sigma$  for step-change in dimensionless relative shear strain amplitude: (a)  $\hat{\gamma} = 2-8$  and (b)  $\hat{\gamma} = 2-500$  for the monolayer with 0% FBS and 10% FBS.

#### IV. DISCUSSION AND CONCLUSIONS

Serum starvation is a standard procedure in cell biology,<sup>32</sup> but its effect on mechanical or rheological properties of the cells has not been extensively studied. Miyaoka *et al.*<sup>35</sup> reported the micro-rheological properties of serum-starved 3T3 fibroblasts using AFM. They starved the cells at 0.1% FBS for 24 h and conducted the AFM study on single fibroblasts cells in a micro-fabricated glass substrate, whereas, in our study, we report the macro-rheological properties of cell monolayer with and without serum at 10% and 0% FBS, respectively. Our study has shown a significant difference in the rheology of the cell monolayer for both the cases: (a) with serum (10% FBS) and (b) without serum (0% FBS) as well as at (a) low shear strain and (b) high shear strain. We can infer that the rheological properties of the cell monolayer depend on shear strain and concentration of serum in growth media. The experiments were conducted by placing the cell monolayer between two parallel plates.

First, in the oscillatory amplitude sweep experiments, we found that for low dimensionless relative shear strain ( $\hat{\gamma}$ ), cell monolayer behaves like an elastic solid and both moduli,  $G'$  and  $G''$ , remain constant for cell monolayer with and without-serum. As the strain is increased, interestingly, both storage and loss moduli decrease, and after a certain strain value, loss modulus ( $G''$ ) becomes larger than the storage modulus indicating the transition from an elastic solid-like to the viscous fluid-like behavior of the cell monolayer. The non-linear viscoelastic moduli show a slight difference at higher strains, but the trend remains the same as linear moduli for both serum-starved and healthy cell monolayers (Fig. 5). Our storage and loss moduli values are consistent with the data of Dakhil *et al.*<sup>13</sup> on HeLa cells at the gap of 15  $\mu\text{m}$ .

The transition from an elastic solid-like to the viscous fluid-like behavior in a cell monolayer is attributed to the dynamic nature of the cytoskeleton of its cells.<sup>29,49</sup> This transition also depends on the applied frequency of the oscillatory strain. Our study shows that the crossover of  $G'$  and  $G''$  is delayed as the frequency is increased. This effect is more prominent for serum-free cell monolayer (Fig. 6). Detailed analysis is required to understand the non-linear behavior of healthy and serum-starved cell monolayers at different frequencies.

Our results show the strain-softening of the cell monolayer similar to many other studies on cells,<sup>29,50</sup> in contrast to studies that report strain-stiffening.<sup>51–53</sup> This paradox of strain stiffening and softening was studied by Wolff *et al.*<sup>54</sup> on minimal cytoskeleton model system [F-actin/heavy meromyosin (HMM)], which shows similar softening-stiffening behavior. They proposed that the stiffening is a direct viscoelastic response to applied stress and caused by the non-linear stretch resistance of individual semiflexible biopolymers, whereas the softening is characterized as inelastic fluidization, which is caused by the dynamical evolution of the mutual bonds between the biopolymers due to the applied strain. In our work, we believe that softening emerges as the characteristic response to the applied strain because of the evolution of the bonds between the biopolymers and cell-cell contacts in the monolayer. Our results also show the soft glassy behavior of the cell monolayers (Fig. 7). The soft glassy nature for the healthy cell monolayer with 10% FBS [Fig. 7(b)] is more pronounced than for the starved cell monolayer [Fig. 7(a)], again confirming that in the absence of the serum, the cell monolayer loses the ability to restructure itself.

The LAOS experiments also show a significant difference between cell monolayer's behavior for healthy and serum-starved cell

monolayers. The onset of non-linearity is earlier, as shown by elastic Lissajous–Bowditch curves (Fig. 11) for serum-free cell monolayer (0% FBS). The cell monolayer shows the shear softening (similar to weak strain overshoot<sup>43,44</sup>) in amplitude sweep experiments. We have also used fibronectin to control the slip at the upper plate. The cell monolayer with 0% FBS shows the stronger effect of fibronectin adhesion, whereas we did not observe much effect of adhesion on the healthy cell monolayer (10% FBS) as shown in Fig. 9.

In frequency sweep experiments, our findings suggest that for small deformation in the linear viscoelastic regime, the cell monolayer with and without serum shows weak power-law dependence on the applied frequency. Our observation of macro-rheological storage modulus ( $G'$ ) and loss modulus ( $G''$ ) of the cell monolayer without serum at 0% FBS for the small deformation ( $\hat{\gamma} = 5$ ) in linear viscoelastic regime shows a weak power-law dependence with an exponent “ $s = 0.15$ ” and “ $s = 0.14$ ” throughout the applied frequencies range, respectively. However, for healthy cell monolayer with 10% FBS, only the storage modulus ( $G'$ ) shows the weak power-law dependence ( $s = 0.13$ ) throughout the applied frequency range, whereas the loss modulus ( $G''$ ) shows weak dependence ( $s = 0.13$ ) for low frequencies ( $\omega \leq 20$  rad/s) and a slightly stronger power-law dependence with an exponent “ $s = 0.27$ ” at higher frequencies ( $\omega \geq 20$  rad/s).

In the non-linear viscoelastic regime, at high deformations with  $\hat{\gamma} = 500$  and 5000, serums starved cell monolayer shows a strong power-law dependency for high frequency  $\{\omega \geq 20$  rad/s [Figs. 13(a) and 14(a)]. This indicates that serum-starved monolayer becomes stiff at the large values of strains at high frequency, whereas the cell monolayer with full serum at 10% FBS remains flexible even at the large values of strain and at high frequencies, as power-law dependency remains weak for the cell monolayer with 10% FBS [Figs. 13(b) and 14(b)].

Our results are consistent with Kollmannsberger and Fabry.<sup>17</sup> They showed that the frequency response of the cells follows a weak power-law over a large range of frequencies irrespective of cell type or experimental technique. Miyaoka *et al.*<sup>35</sup> reported the micro-rheological properties of serum-starved NIH3T3 fibroblasts using AFM. They reported the weak power-law dependence of  $G'$  on frequency for serum-starved cells, a common characteristic of many other different types of cells. In our study, at the macroscopic level, for serum-starved cell monolayer at 0% FBS, we observe the weak power-law behavior of  $G'$  and  $G''$  at lower frequencies which becomes more pronounced at higher frequencies, especially in the non-linear viscoelastic regime [Figs. 13(a) and 14(a)]. We can infer that, under serum starvation, macro- and micro-storage modulus tends to show a similar frequency dependence.

Next, we performed the step-change in strain amplitude experiments to study the recovery of applied deformation to the cell monolayer. Our study reveals that a healthy cell monolayer with 10% FBS shows a complete recovery of storage and loss moduli even at large deformation {step-change in dimensionless relative shear strain amplitude from  $\hat{\gamma} = 2$  to 500 [Fig. 17(b)]}, whereas a starving cell monolayer does not recover completely even for small deformations in linear viscoelastic regime {(step-change in strain amplitude from  $\hat{\gamma} = 2$  to 8 [Fig. 16(a)]}. Also, the stress in healthy cell monolayer increases with a very low gradient during the small deformation, but the stress in the serum-free cell monolayer shoots up instantly at a much higher value and then decreases with steep gradient during the step-change in

strain amplitude Fig. 19(a). For high step-change in dimensionless relative shear strain amplitude with  $\hat{\gamma} = 500$ , the stress in a healthy cell monolayer is higher than that of the serum-free cell monolayer. In both cases, stress decreases during the applied step-change in  $\hat{\gamma}$  and recovers instantly when the step-change in strain amplitude was removed. The stress shows a slight decrease in values for the serum-free cell monolayer after the step-change in  $\hat{\gamma}$ . This observation shows that a healthy cell monolayer can distribute stress more effectively than that of the serum-free or starved cell monolayer. This may be because of the many dynamic protein filaments in the cell cytoskeleton, such as the actomyosin network, microtubules, and intermediate filaments responsible for rigidity and restructuring of the cells, redistributing the stress effectively in the cytoskeleton and throughout the cell monolayer, whereas, in the starving cell monolayer, the cell cytoskeleton may not form these fibrous proteins and cannot distribute the stress effectively. Harris *et al.*<sup>55</sup> have shown that the monolayer mechanical properties are strongly dependent on the actin cytoskeleton, myosin, and intercellular adhesions interfacing adjacent cells. In their study, they harvested the cell monolayer and did the stretching experiments to access the mechanical properties of the monolayer. Their study revealed the role of keratin filaments in cell monolayer mechanics. Another study, by Helfand *et al.*,<sup>56</sup> shows that serum starvation has a significant effect on vimentin intermediate filaments organization and strongly affects the lamellipodia formation 3T3 fibroblasts.

Our study reveals that serum starvation leads to significant changes in the cell monolayer's rheological properties. The slip at the walls is also more pronounced for serum-free cell monolayer. These changes may be caused by the lack of the available nutrients for the cells' cytoskeleton, which helps the cells and the monolayer as a whole to reorient and restructure itself in the direction of the applied strain. Serum starvation leads to reduced protein synthesis and degraded cell growth.<sup>32,56</sup> This leads to less active cells with a less dynamic cytoskeleton of the cells. In the absence of serum, which contains all the nutrients and growth factors, cells become less active, and its cytoskeleton does not effectively restructure itself in response to the applied strain. In our experiments, we have shown that the cell monolayer, under serum-free conditions, appears to be softer than the monolayer, which is supplied with all the nutrients and growth factor, i.e., with 10% FBS. In the presence of serum, cells are healthy and more dynamic or active and can effectively restructure their cytoskeleton under a given strain or stress. This leads to its increased strength and more dynamic behavior.

## SUPPLEMENTARY MATERIAL

See the [supplementary material](#) for the detailed experimental protocol and additional imaging and video data to validate the constant gap between the parallel plates.

## ACKNOWLEDGMENTS

We acknowledge Professor J. W. Nelson for sending the MDCK cell line. The authors acknowledge the support from the Science and Engineering Research Board, Department of Science & Technology, (SERB-DST) Grant No. CRG/2020/003342 funded by Government of India.

## DATA AVAILABILITY

The data that support the findings of this study are available within the article and its [supplementary material](#).

## REFERENCES

- B. Fregin, F. Czerwinski, D. Biedenweg, S. Girardo, S. Gross, K. Aurich, and O. Otto, "High-throughput single-cell rheology in complex samples by dynamic real-time deformability cytometry," *Nat. Commun.* **10**, 1–11 (2019).
- G. Massiera, K. M. Van Citters, P. L. Biancaniello, and J. C. Crocker, "Mechanics of single cells: Rheology, time dependence, and fluctuations," *Biophys. J.* **93**, 3703–3713 (2007).
- M. Sander, J. Flesch, and A. Ott, "Using cell monolayer rheology to probe average single cell mechanical properties," *Biorheology* **52**, 269–278 (2015).
- E. J. McDowell, A. K. Ellerbee, M. A. Choma, B. E. Applegate, and J. A. Izatt, "Spectral domain phase microscopy for local measurements of cytoskeletal rheology in single cells," *J. Biomed. Opt.* **12**, 044008 (2007).
- S. Hiratsuka, Y. Mizutani, M. Tsuchiya, K. Kawahara, H. Tokumoto, and T. Okajima, "The number distribution of complex shear modulus of single cells measured by atomic force microscopy," *Ultramicroscopy* **109**, 937–941 (2009).
- B. Lincoln, F. Wottawah, S. Schinkinger, S. Ebert, and J. Guck, "High-throughput rheological measurements with an optical stretcher," in *Cell Mechanics, Methods in Cell Biology*, Vol. 83 (Academic Press, 2007), pp. 397–423.
- F. Wottawah, S. Schinkinger, B. Lincoln, R. Ananthakrishnan, M. Romeyke, J. Guck, and J. Käs, "Optical rheology of biological cells," *Phys. Rev. Lett.* **94**, 098103 (2005).
- B. R. Brückner, H. Nöding, and A. Janshoff, "Viscoelastic properties of confluent MDCK II cells obtained from force cycle experiments," *Biophys. J.* **112**, 724–735 (2017).
- S. Nehls, H. Nöding, S. Karsch, F. Ries, and A. Janshoff, "Stiffness of MDCK II cells depends on confluency and cell size," *Biophys. J.* **116**, 2204–2211 (2019).
- B. R. Brückner and A. Janshoff, "Importance of integrity of cell-cell junctions for the mechanics of confluent MDCK II cells," *Sci. Rep.* **8**, 1–11 (2018).
- D. T. N. Chen, Q. Wen, P. A. Janmey, J. C. Crocker, and A. G. Yodh, "Rheology of soft materials," *Annu. Rev. Condens. Matter Phys.* **1**(1), 301–322 (2010).
- P. Fernandez, L. Heymann, A. Ott, N. Aksel, and P. A. Pullarkat, "Shear rheology of a cell monolayer," *New J. Phys.* **9**, 419 (2007).
- H. Dakhil, D. F. Gilbert, D. Malhotra, A. Limmer, H. Engelhardt, A. Amtmann, J. Hansmann, H. Hübner, R. Buchholz, O. Friedrich, and A. Wierschem, "Measuring average rheological quantities of cell monolayers in the linear viscoelastic regime," *Rheol. Acta* **55**, 527–536 (2016).
- F. G. Schmidt, B. Hinner, and E. Sackmann, "Microrheometry underestimates the values of the viscoelastic moduli in measurements on F-actin solutions compared to macrorheometry," *Phys. Rev. E* **61**, 5646 (2000).
- W. J. Weigand, A. Messmore, J. Tu, A. Morales-Sanz, D. L. Blair, D. D. Deheyn, J. S. Urbach, and R. M. Robertson-Anderson, "Active microrheology determines scale-dependent material properties of *Chaetopterus mucus*," *PLoS One* **13**, e0203102 (2018).
- E. H. Zhou, F. D. Martinez, and J. J. Fredberg, "Mush rather than machine," *Nat. Mater.* **12**, 184–185 (2013).
- P. Kollmannsberger and B. Fabry, "Linear and nonlinear rheology of living cells," *Annu. Rev. Mater. Res.* **41**, 75–97 (2011).
- B. Fabry, G. Maksym, J. Butler, M. Glogauer, D. Navajas, and J. Fredberg, "Scaling the microrheology of living cells," *Phys. Rev. Lett.* **87**, 148102 (2001).
- D. Stamenovic, B. Suki, B. Fabry, N. Wang, J. J. Fredberg, and J. E. Buy, "Rheology of airway smooth muscle cells is associated with cytoskeletal contractile stress," *J. Appl. Physiol.* **96**, 1600–1605 (2004).
- B. Fabry, G. N. Maksym, J. P. Butler, M. Glogauer, D. Navajas, N. A. Taback, E. J. Millet, and J. J. Fredberg, "Time scale and other invariants of integrative mechanical behavior in living cells," *Phys. Rev. E* **68**, 041914 (2003).
- N. Rosenblatt, S. Hu, J. Chen, N. Wang, and D. Stamenovic, "Distending stress of the cytoskeleton is a key determinant of cell rheological behavior," *Biochem. Biophys. Res. Commun.* **321**, 617–622 (2004).
- X. Trepas, M. Grabulosa, F. Puig, G. N. Maksym, D. Navajas, and R. Farré, "Viscoelasticity of human alveolar epithelial cells subjected to stretch," *Am. J. Physiol.: Lung Cell. Mol. Physiol.* **287**, L1025–L1034 (2004).

- <sup>23</sup>D. Stamenovic, "Rheological behavior of mammalian cells," *Cell. Mol. Life Sci.* **65**, 3592–3605 (2008).
- <sup>24</sup>D. Ingber, "Tensegrity I. Cell structure and hierarchical systems biology," *J. Cell Sci.* **116**, 1157–1173 (2003).
- <sup>25</sup>D. E. Ingber, N. Wang, and D. Stamenovic, "Tensegrity, cellular biophysics, and the mechanics of living systems," *Rep. Prog. Phys.* **77**, 046603 (2014).
- <sup>26</sup>G. Lenormand, E. Millet, B. Fabry, J. P. Butler, and J. J. Fredberg, "Linearity and time-scale invariance of the creep function in living cells," *J. R. Soc., Interface* **1**, 91–97 (2004).
- <sup>27</sup>L. Deng, X. Trepap, J. P. Butler, E. Millet, K. G. Morgan, D. A. Weitz, and J. J. Fredberg, "Fast and slow dynamics of the cytoskeleton," *Nat. Mater.* **5**, 636–640 (2006).
- <sup>28</sup>P. Bursac, G. Lenormand, B. Fabry, M. Oliver, D. Weitz, V. Viasnoff, J. Butler, and J. Fredberg, "Cytoskeletal remodeling and slow dynamics in the living cell," *Nat. Mater.* **4**, 557–561 (2005).
- <sup>29</sup>X. Trepap, L. Deng, S. S. An, D. Navajas, D. J. Tschumperlin, W. T. Gerthoffer, J. P. Butler, and J. J. Fredberg, "Universal physical responses to stretch in the living cell," *Nature* **447**, 592–595 (2007).
- <sup>30</sup>N. Rosenblatt, A. M. Alencar, A. Majumdar, B. Suki, and D. Stamenovic, "Dynamics of prestressed semiflexible polymer chains as a model of cell rheology," *Phys. Rev. Lett.* **97**, 168101 (2006).
- <sup>31</sup>K. Kroy and J. Glaser, "The glassy wormlike chain," *New J. Phys.* **9**, 416 (2007).
- <sup>32</sup>S. Pirkmajer and A. V. Chibalin, "Serum starvation: Caveat emptor," *Am. J. Physiol.* **301**, C272–C279 (2011).
- <sup>33</sup>G. M. Cooper, *The Cell: A Molecular Approach*, 8th ed. (Oxford University Press, 2018).
- <sup>34</sup>J. K. Wróbel, R. Cortez, and L. Fauci, "Modeling viscoelastic networks in Stokes flow," *Phys. Fluids* **26**, 113102 (2014).
- <sup>35</sup>A. Miyaoka, Y. Mizutani, M. Tsuchiya, K. Kawahara, and T. Okajima, "Rheological properties of growth-arrested fibroblast cells under serum starvation measured by atomic force microscopy," *Jpn. J. Appl. Phys., Part 1* **50**, 08LB16 (2011).
- <sup>36</sup>F. Drees, S. Pokutta, S. Yamada, W. J. Nelson, and W. I. Weis, "Alpha-catenin is a molecular switch that binds E-cadherin-beta-catenin and regulates actin-filament assembly," *Cell* **123**, 903–915 (2005).
- <sup>37</sup>A. Hartsock and W. J. Nelson, "Adherens and tight junctions: Structure, function and connections to the actin cytoskeleton," *Biochim. Biophys. Acta* **1778**, 660–669 (2008).
- <sup>38</sup>S. Tavares, A. F. Vieira, A. V. Taubenberger, M. Araújo, N. P. Martins, C. Brás-Pereira, A. Polónia, M. Herbig, C. Barreto, O. Otto, J. Cardoso, J. B. Pereira-Leal, J. Guck, J. Paredes, and F. Janody, "Actin stress fiber organization promotes cell stiffening and proliferation of pre-invasive breast cancer cells," *Nat. Commun.* **8**, 1–18 (2017).
- <sup>39</sup>R. H. Ewoldt, "Defining nonlinear rheological material functions for oscillatory shear," *J. Rheol.* **57**, 177 (2013).
- <sup>40</sup>R. H. Ewoldt, A. E. Hosoi, and G. H. McKinley, "New measures for characterizing nonlinear viscoelasticity in large amplitude oscillatory shear," *J. Rheol.* **52**, 1427 (2008).
- <sup>41</sup>S. A. Rogers and M. P. Lettinga, "A sequence of physical processes determined and quantified in large-amplitude oscillatory shear (LAOS): Application to theoretical nonlinear models," *J. Rheol.* **56**, 1 (2012).
- <sup>42</sup>I. Argatov, A. Iantchenko, and V. Kocherbitov, "How to define the storage and loss moduli for a rheologically nonlinear material?," *Continuum Mech. Thermodyn.* **29**, 1375–1387 (2017).
- <sup>43</sup>K. Hyun, S. H. Kim, K. H. Ahn, and S. J. Lee, "Large amplitude oscillatory shear as a way to classify the complex fluids," *J. Non-Newtonian Fluid Mech.* **107**, 51–65 (2002).
- <sup>44</sup>K. Hyun, M. Wilhelm, C. O. Klein, K. S. Cho, J. G. Nam, K. H. Ahn, S. J. Lee, R. H. Ewoldt, and G. H. McKinley, "A review of nonlinear oscillatory shear tests: Analysis and application of large amplitude oscillatory shear (LAOS)," *Prog. Polym. Sci.* **36**, 1697–1753 (2011).
- <sup>45</sup>H. G. Sim, K. H. Ahn, and S. J. Lee, "Large amplitude oscillatory shear behavior of complex fluids investigated by a network model: A guideline for classification," *J. Non-Newtonian Fluid Mech.* **112**, 237–250 (2003).
- <sup>46</sup>M. Kamkar, M. Janmaleki, E. Erfanian, A. Sanati-Nezhad, and U. Sundararaj, "Viscoelastic behavior of covalently crosslinked hydrogels under large shear deformations: An approach to eliminate wall slip," *Phys. Fluids* **33**, 041702 (2021).
- <sup>47</sup>T. B. Goudoulas, S. Pan, and N. Germann, "Nonlinearities and shear banding instability of polyacrylamide solutions under large amplitude oscillatory shear," *J. Rheol.* **61**, 1061 (2017).
- <sup>48</sup>S. Rogers, "Large amplitude oscillatory shear: Simple to describe, hard to interpret," *Phys. Today* **71**(7), 34–40 (2018).
- <sup>49</sup>D. Stamenovic, "Effects of cytoskeletal prestress on cell rheological behavior," *Acta Biomater.* **1**, 255–262 (2005).
- <sup>50</sup>R. Krishnan, C. Y. Park, Y.-C. Lin, J. Mead, R. T. Jaspers, X. Trepap, G. Lenormand, D. Tambe, A. V. Smolensky, A. H. Knoll, J. P. Butler, and J. J. Fredberg, "Reinforcement versus fluidization in cytoskeletal mechanoresponsiveness," *PLoS One* **4**, e5486 (2009).
- <sup>51</sup>J. Pourati, A. Maniotis, D. Spiegel, J. L. Schaffer, J. P. Butler, J. J. Fredberg, D. E. Ingber, D. Stamenovic, and N. Wang, "Is cytoskeletal tension a major determinant of cell deformability in adherent endothelial cells?," *Am. J. Physiol.: Cell Physiol.* **274**, 1283–1289 (1998).
- <sup>52</sup>N. Wang, I. M. Tolić-Nørrelykke, J. Chen, S. M. Mijailovich, J. P. Butler, J. J. Fredberg, and D. Stamenovic, "Cell prestress. I. Stiffness and prestress are closely associated in adherent contractile cells," *Am. J. Physiol.: Cell Physiol.* **282**, C606–C616 (2002).
- <sup>53</sup>P. Fernandez, P. A. Pullarkat, and A. Ott, "A master relation defines the nonlinear viscoelasticity of single fibroblasts," *Bioophys. J.* **90**, 3796–3805 (2006).
- <sup>54</sup>L. Wolff, P. Fernandez, and K. Kroy, "Resolving the stiffening-softening paradox in cell mechanics," *PLoS One* **7**, e40063 (2012).
- <sup>55</sup>A. R. Harris, L. Peter, J. Bellis, B. Baum, A. J. Kabla, and G. T. Charras, "Characterizing the mechanics of cultured cell monolayers," *Proc. Natl. Acad. Sci. U. S. A.* **109**, 16449–16454 (2012).
- <sup>56</sup>B. T. Helfand, M. G. Mendez, S. N. P. Murthy, D. K. Shumaker, B. Grin, S. Mahammad, U. Aebi, T. Wedig, Y. I. Wu, K. M. Hahn, M. Inagaki, H. Herrmann, and R. D. Goldman, "Vimentin organization modulates the formation of lamellipodia," *Mol. Biol. Cell* **22**, 1274–1289 (2011).